

# Understanding Hadron Structure Using Lattice QCD

J.W. NEGELE

*Center for Theoretical Physics*

*Laboratory for Nuclear Science and Department of Physics*

*Massachusetts Institute of Technology, Cambridge MA 02139*

**Abstract** An elementary introduction is presented to the study of hadron structure using lattice QCD. Following a brief review of relevant aspects of path integrals, the discrete lattice path integral is presented for gluon and quark fields and used to calculate physical observables. Essential aspects of instanton physics are reviewed, and it is shown how the instanton content is extracted from lattice gluon configurations. Finally, both comparison of results including all gluons with those including only instantons and the study of quark zero modes associated with instantons and their contributions to hadronic observables are used to show the dominant role of gluons in hadron structure. MIT CTP# 2701 hep-lat/9804017

## 1. – Introduction and Motivation

Although a quarter of a century has passed since the experimental discovery of quarks and the formulation of QCD, we are only now beginning to understand the essential physics of the structure of light hadrons. To truly understand hadron structure, one must solve rather than model QCD, and the only known means to do so is the numerical solution of lattice field theory. But obtaining accurate numerical results for observables from a computer is not enough — we also need to obtain physical insight. Hence, our strategy is to use numerical evaluation of the QCD path integral on a lattice to identify the configurations that dominate the action as well as to calculate observables. In recent years, the algorithms and techniques of lattice QCD and the performance of massively parallel computers have developed to the point that we are now on the threshold of reliable, quantitative calculations of QCD observables. Furthermore, there is strong evidence from lattice calculations that the topological excitations of the gluon field corresponding in the semiclassical limit to instantons play a dominant role in the structure of light hadrons. The purpose of these lectures is to describe at an elementary level the basic elements of lattice QCD and how numerical solution of QCD on a lattice is elucidating the role of instantons in light hadrons.

To appreciate the significance of the current lattice results, it is useful to recall the wide range of disparate physical pictures that have arisen from the different QCD inspired models introduced to model hadrons. For example, non-relativistic quark models focus on constituent quarks interacting via an adiabatic potential. Bag models postulate a

region in which relativistic current quarks are confined and interact by gluon exchange. Motivated by large  $N_c$  arguments, Skyrme models describe the nucleon as a topological soliton built out of  $q\bar{q}$  pairs. Finally instanton models emphasize the role of topological excitations of the vacuum and of the quark zero modes associated with these excitations.

Unfortunately, phenomenology has proven inconclusive in determining which, if any, of these fundamentally different pictures describes the essential physics of light hadrons, since each of the models is rich enough that with sufficient embellishment it can be made to fit much of the data. Whereas perturbative QCD has proven extremely useful in extracting quark and gluon structure functions from high energy scattering experiments, it is inadequate to understand their origin. Hence, it is necessary to turn to nonperturbative solution of QCD on the lattice.

The physical picture that arises from this work corresponds closely to the physical arguments and instanton models of Shuryak and others [1, 2, 3] in which the zero modes associated with instantons produce localized quark states, and quark propagation proceeds primarily by hopping between these states. Thus, QCD with light quarks is unique among the many-body systems with which we are familiar in the sense that the quanta generating the interactions cannot be subsumed into a potential but rather participate as essential dynamical degrees of freedom. In atoms, for example, photons play a negligible dynamical role, and to an excellent approximation may be subsumed into the static Coulomb potential. In nuclei, mesons play a minor dynamical role, and to a good approximation nuclear structure maybe described in terms of two- and three-body nuclear forces. Indeed, experimentalists need to work very hard and pick their cases carefully to observe any effects of meson exchange currents. And in heavy quark systems, much of the physics of  $c\bar{c}$  and  $b\bar{b}$  bound states may be understood by subsuming the gluons into an adiabatic potential with Coulombic and confining behavior. The fact that nucleons are completely different in that gluons are crucial dynamical degrees of freedom is not entirely unexpected. Indeed, from perturbative QCD, we already know by the work of Gross and Wilczek [4] and Hoodbhoy, Ji, and Tang [5] that approximately half ( $16/3n_f$  to be precise, where  $n_f$  is the number of active flavors and equals 5 below the top quark mass) of the momentum and angular momentum comes from glue in the limit of high  $Q^2$ . Furthermore, experiment tells us that this behavior continues down to non-perturbative scales of the order of several  $\text{GeV}^2$ .

The discussion of lattice QCD will be based on four key, underlying ideas. The first is the use of path integrals. One of the great contributions of Feynman to theoretical physics was the formulation of quantum mechanics in terms of path integrals, which provides both a physical picture of quantum evolution in terms of sums of time histories and a powerful computational framework. For the present application, we will make use of the fact that the path integral eliminates the non-commuting operators of quantum mechanics or field theory by introducing an integral over an additional continuous variable, and thus effectively reduces the problem of quadrature.

The second major idea is the introduction of Euclidean time. The basic idea is to write  $|\psi\rangle = e^{-\beta H}|\phi\rangle$ , where  $e^{-\beta H}$  acts as a filter to project the ground state  $|\psi\rangle$  out of an arbitrary state  $|\phi\rangle$  having the desired set of quantum numbers, so the continuous

variable in the path integral is imaginary or Euclidean time. The resulting theory has important connections with statistical mechanics. In the case in which one sums over a complete set of states and calculates the trace  $\text{Tr } e^{-\beta H}$ , one is solving field theory at finite temperature and  $\beta$  corresponds to the physical inverse temperature. The corresponding path integral has the structure of classical statistical mechanics in  $d+1$  dimensions. Many familiar ideas from statistical physics concerning critical behavior, order parameters, and Landau's theory of phase transition turn out to be useful.

The third principal idea is lattice regularization, which replaces continuum field theory by a finite quantum many-body problem on a lattice. For any finite lattice spacing  $a$ , the maximum momentum which can arise on the lattice is  $p_{\text{max}} \sim \frac{\pi}{a}$ , so that the lattice effectively imposes a momentum cutoff of order  $p_{\text{max}}$  which goes to infinity as the lattice spacing goes to zero. One of the great accomplishments in recent years has been the use of renormalization group arguments and other techniques to provide convincing approximation to the underlying continuum theory.[7]

The last key idea is the use of stochastic, or Monte Carlo, methods to evaluate the lattice path integrals. One should note at the outset that the common misnomer of Monte Carlo "simulations" is quite misleading. In fact, we are not simulating anything. Rather, we are solving an equation in the same sense as one always uses numerical analysis to solve equations. That is, one first selects a desired level of precision, and then using appropriate theorems, determines an algorithm and a number of independent samples which yields that precision.

The outline of these lectures is as follows. Following this introduction, aspects of path integrals relevant to lattice QCD are reviewed in Section 2. The basic ideas of lattice QCD are presented beginning with the pure gluon sector in Section 3 and then adding quarks in Section 4. The role on instantons in light hadrons is discussed in the final section. Following an overview of instantons, it is shown how the instanton content is extracted from lattice gluon configurations. Results including all gluon contributions are compared with those including only instantons to provide one indication of the dominant role of instantons. Finally, direct calculation of quark zero modes, observation of quark localization for these modes at the locations of instantons, and demonstration that these modes dominate the rho and pion contributions to vector and pseudoscalar correlation functions provide additional indications of the role of instantons in hadron structure.

For readers who wish to go beyond the scope of the present lecture, I recommend several basic references. Much of the background material is discussed in more detail in a text co-authored with Orland.[8] In particular, the reader is referred to Chapter 1 for treatment of coherent states and Grassmann variables, Chapter 2 for discussion of path integrals, and Chapter 8 for a detailed explanation of stochastic methods. A terse introduction to lattice gauge theory is provided by Creutz [9] and more details may be found in the reprint volume edited by Rebbi [10] which includes all the key articles through 1983 and in comprehensive texts written by Rothe [11] and by Montvay and Münster [12]. Up-to-date reviews of recent results may be found in the proceedings of the yearly lattice conferences published in *Nuclear Physics B* Proceedings Supplements.

## 2. – Path Integrals

**2.1. Feynman Path Integral.** – The basic idea of the path integral is illustrated by considering the Feynman path integral for a single degree of freedom. The evolution operator  $e^{-iHt}$  is broken up into a large number of “time slices” separated by time interval  $\epsilon$ , and a complete set of states is inserted between each interval

$$(2.1) \quad e^{-iHt} = e^{-iH\epsilon} \int dx_n |x_n\rangle \langle x_n| e^{-iH\epsilon} \int dx_{n-1} |x_{n-1}\rangle \langle x_{n-1}| e^{-iH\epsilon} \dots$$

Then, the non-commutativity of the kinetic and potential energy operators is treated by the following approximation which becomes exact in the limit  $\epsilon \rightarrow 0$

$$(2.2) \quad \begin{aligned} \langle x_{k+1} | e^{-i\epsilon \left( \frac{\hat{p}^2}{2m} + V(\hat{x}) \right)} | x_k \rangle &\sim \langle x_{k+1} | e^{-i\epsilon \frac{\hat{p}^2}{2m}} \int dp |p\rangle \langle p| e^{-i\epsilon V(\hat{x})} | x_k \rangle \\ &= \int dp e^{ip(x_{k+1}-x_k) - i\epsilon \frac{p^2}{2m} - i\epsilon V(x_k)} \\ &= \sqrt{\frac{2m\pi}{\epsilon}} e^{i\epsilon \sum_k \left[ \frac{m}{2} \left( \frac{x_{k+1}-x_k}{\epsilon} \right)^2 - V(x_k) \right]} + \mathcal{O}(\epsilon^2) \end{aligned}$$

Hence the evolution operator may be expressed as the sum over all paths of the exponential of the classical action

$$(2.3) \quad \begin{aligned} \langle x_f | e^{-iHt} | x_i \rangle &= \int \mathcal{D}(x_1, \dots, x_n) e^{i\epsilon \sum_k \left[ \frac{m}{2} \left( \frac{x_{k+1}-x_k}{\epsilon} \right)^2 - V(x_k) \right]} \\ &\rightarrow \int_{x(0)=x_i}^{x(t)=x_f} \mathcal{D}(x_1, \dots, x_n) e^{i\epsilon S_{\text{classical}}(x(t))} \end{aligned}$$

The quantum mechanics of the non-commuting operators  $\hat{x}$  and  $\hat{p}$  has thus been represented by an ordinary integral over an additional time variable. This result may be generalized to many degrees of freedom as follows

$$(2.4) \quad \langle x_1^f \dots x_N^f | e^{-iHt} | x_1^i \dots x_N^i \rangle = \int_{x_1^i \dots x_N^i}^{x_1^f \dots x_N^f} e^{i\epsilon \sum_k \left[ \sum_i \frac{m}{2} \left( \frac{x_i^{k+1}-x_i^k}{\epsilon} \right)^2 - \frac{1}{2} \sum_{ij} v(x_i^k - x_j^k) \right]}$$

where a complete set of states  $|x_1 \dots x_N\rangle \langle x_1 \dots x_N|$ , is inserted at each time slice.

One important property of the path integral is that a time-ordered product is represented as follows:

$$(2.5) \quad \begin{aligned} T \mathcal{O}(t_1) \mathcal{O}(t_2) e^{-i \int_0^T dt H(t)} &= e^{-iH(T-t_2)} \mathcal{O}(t_2) e^{-iH(t_2-t_1)} \mathcal{O}(t_1) e^{-iH(t_1-0)} \\ &\rightarrow \int \mathcal{D}(x_1, \dots, x_n) e^{iS(x_1, \dots, x_n)} \mathcal{O}(x_{k_2}) \mathcal{O}(x_{k_1}) \end{aligned}$$

Hence, any path integral composed of  $e^{iS}$  and a sequence of operators automatically corresponds to a time-ordered product.

The classical limit is obtained by including the factors of  $\hbar$  which have been suppressed thus far and applying the stationary phase approximation

$$(2.6) \quad \int \mathcal{D}(x) e^{\frac{i}{\hbar} S(x)} \xrightarrow{\text{SPA}} e^{\frac{i}{\hbar} S(x_{cl})} \left( \frac{1}{\sqrt{\det \left( m \frac{d^2}{dt^2} + V''(x_0(t)) \right)}} + \mathcal{O}(\hbar) \right)$$

in which case the path integral represents the sum of all quadratic fluctuations around the classical path.

It is important to note that there is nothing sacred about the physical time, and any continuous variable may be “sliced” to treat the non-commutativity of  $\hat{x}$  and  $\hat{p}$ . A common case is the Euclidean path integral, in which real time is replaced by imaginary time or temperature, with the result

$$(2.7) \quad e^{-\beta H} = \prod e^{-\epsilon H} \implies \int \mathcal{D}(x) e^{-\sum_k \epsilon \left[ \frac{m}{2} \left( \frac{x_{k+1} - x_k}{\epsilon} \right)^2 + V(x_k) \right]}$$

In this analytic continuation in which  $it \rightarrow \tau$ , the Lagrangian is effectively replaced by the Hamiltonian in the exponent

$$(2.8) \quad \int dt \left[ \frac{m}{2} \dot{x}^2 - V \right] \xrightarrow{it \rightarrow \tau} \int d\tau \left[ \frac{m}{2} \dot{x}^2 + V \right]$$

Salient properties of this Euclidean path integral are the fact that it is purely real, it has a well-defined measure, the Wiener measure, and it has the structure of the partition function of statistical mechanics with one extra dimension.

The boundary conditions on the path integral are specified by the specific matrix element or elements under consideration. For example, the thermodynamic trace has the form

$$(2.9) \quad \text{Tr} e^{-\beta H} = \int dx \langle x | e^{-\beta H} | x \rangle = \int \mathcal{D}(x_0, x_1, \dots, x_n) e^{-S(x_0, \dots, x_n)}$$

where

$$(2.10) \quad S(x_0, \dots, x_n) = \epsilon \left[ \frac{m}{2} \frac{(x_0 - x_n)^2}{\epsilon^2} + V(x_n) + \frac{m}{2} \frac{(x_n - x_{n-1})^2}{\epsilon} + V(x_{n-1}) \right. \\ \left. + \dots + \frac{m}{2} \frac{(x_1 - x_0)^2}{\epsilon} + V(x_0) \right]$$

and thus has periodic boundary conditions. For specific matrix elements however, we obtain the alternative form

$$(2.11) \quad \langle \phi_f | e^{-\beta H} | \phi_i \rangle = \int \mathcal{D}(x_0, x_1, \dots, x_n, x_{n+1}) e^{-S(x_0, \dots, x_{n+1})}$$

where

$$(2.12) \quad S(x_0, \dots, x_{n+1}) = -\ln \phi_f(x_{n+1}) + \epsilon \left[ \frac{m}{2} \left( \frac{x_{n+1} - x_n}{\epsilon} \right)^2 + V(x_n) + \dots \right. \\ \left. + \frac{m}{2} \left( \frac{x_1 - x_0}{\epsilon} \right)^2 + V(x_0) \right] - \ln \phi_i(x_0) .$$

**2.2. Scalar Field Theory.** – Using this knowledge of the Feynman path integral, it is now easy to generalize to scalar field theory on a lattice. Let the continuum coordinate  $\vec{r}$  be replaced by discrete lattice coordinates  $\vec{n} \equiv (n_1, n_2, n_3)$  where the  $n_i$  are integers and lengths will be understood to be in units of the lattice spacing  $a$ . Then one simply views the lattice field theory as a quantum many-body problem where the canonical coordinate and momentum operators  $\hat{x}_i$  and  $\hat{p}_i$  are replaced by  $\hat{\phi}(\vec{n})$  and  $\hat{\pi}(\vec{n})$  and the position eigenstates  $\hat{x}_i|x\rangle = x_i|x\rangle$  are replaced by eigenstates  $\hat{\phi}(\vec{n})|\phi\rangle = \phi(\vec{n})|\phi\rangle$ . On the spatial mesh the Hamiltonian density becomes

$$(2.13) \quad \int d^3r \left\{ \frac{1}{2} \pi^2(r) + \frac{1}{2} |\nabla \phi(r)|^2 + V(\phi) \right\} \\ \Rightarrow \sum_{\vec{n}} \left\{ \frac{1}{2} \pi^2(\vec{n}) + \frac{1}{2} \sum_{i=1}^3 |\phi(\vec{n} + \mu_i) - \phi(\vec{n})|^2 + V(\phi(\vec{n})) \right\}$$

where  $\mu_i$  denotes a displacement by one lattice site in the  $i^{\text{th}}$  direction,  $\sum_{\vec{n}} \frac{1}{2} \pi^2(\vec{n})$  corresponds to the kinetic energy  $\sum_j \frac{1}{2m} \hat{p}_j^2$ , and the remaining terms, which we will denote as  $F[\phi(\vec{n})]$  to avoid confusion with  $V[\phi(n)]$  above, correspond to a sum of one- and two-body potentials  $\sum_{ij} v(\hat{x}_i, \hat{x}_j)$ . Introducing time slices as before yields

$$(2.14) \quad e^{-\beta \sum_{\vec{n}} \left\{ \frac{1}{2} \pi^2(\vec{n}) + F[\phi(\vec{n})] \right\}} = \int \mathcal{D}(\phi_k(\vec{n})) e^{-\sum_{k,\vec{n}} \frac{1}{2} (\phi_{k+1}(\vec{n}) - \phi_k(\vec{n}))^2 + F[\phi_k(\vec{n})]}$$

The result is a path integral defined on a four-dimensional lattice, for which we may introduce the obvious notation  $n = (n_0, n_1, n_2, n_3)$  where  $n_0$  denotes the time label and  $n_i$  denotes the spatial label. One observes that time slicing replaces  $\hat{\pi}(\vec{n})$  by  $|\phi_{k+1}(\vec{n}) - \phi_k(\vec{n})|^2 \equiv |\phi(n + \mu_0) - \phi(n)|^2$  which has the same structure as the discrete spatial derivative  $|\nabla \phi|^2 = \sum_{i=1}^3 |\phi(n + \mu_i) - \phi(n)|^2$ . Hence, a general time-ordered product acquires the simple form

$$(2.15) \quad T \mathcal{O}(\phi) e^{-\beta \int d^3r \left\{ \frac{1}{2} \pi^2 + \frac{1}{2} (\nabla \phi)^2 + V(\phi) \right\}} \rightarrow \int \mathcal{D}(\phi(n)) \mathcal{O}(\phi) e^{-S_{\text{Eucl.}}(\phi)}$$

where the Euclidean action is

$$(2.16) \quad S_{\text{Eucl.}}(\phi) \equiv \sum_n \left\{ \frac{1}{2} \sum_{i=0}^3 (\phi(n + \mu_i) - \phi(n))^2 + V(\phi(n)) \right\}$$

This result merits several comments. Note that  $S_{\text{Eucl.}}(\phi)$  is completely symmetric in space and time, even though the first differences in space variables arose from a finite-difference approximation to the spatial derivatives whereas the time differences arose from the path integral time slicing. Of course, we are always free to pick different mesh spacings,  $a_x$  and  $a_t$ , in the space and time directions, respectively. Although in this derivation, we have gone from  $H$  to  $S$  using a discrete transfer matrix for evolution from one time slice to the next, it will often be useful to go backwards in the other direction to think of the lattice action as describing evolution of specific states under the

Hamiltonians  $H$  from one time slice to another in order to interpret lattice observables. Depending on the problem, we may be led to apply different boundary conditions in  $x$  and  $t$ . In the case in which all boundary conditions are periodic, the physical problem corresponds to finite temperature field theory in a periodic three-dimensional box and the shortest side of the four-dimensional box will effectively act as the temperature.

**2.3. Coherent States.** – We now need to generalize this scalar field result for general second quantized Fermion or Boson fields. Recall that the Feynman path integral, and hence the scalar field path integral, used two basic ingredients: eigenstates of  $\hat{x}$ ,  $\hat{x}|x\rangle = x|x\rangle$ , and the resolution of unity,  $1 = \int dx|x\rangle\langle x|$ . The analogs of these relations for creation and annihilation operators are provided by Boson coherent states.

The basic idea is seen most simply for a single creation operator  $\hat{a}^\dagger$ , corresponding to a simple harmonic oscillator, for which

$$\begin{aligned} [\hat{a}, \hat{a}^\dagger] &= 1 \\ \left\{ \begin{array}{c} \hat{a}^\dagger \\ \hat{a} \end{array} \right\} |n\rangle &= \left\{ \begin{array}{c} \sqrt{n+1} \\ \sqrt{n} \end{array} \right\} |n \pm 1\rangle \\ (2.17) \quad |n\rangle &= \frac{1}{\sqrt{n!}} (\hat{a}^\dagger)^n |0\rangle . \end{aligned}$$

The coherent state  $|Z\rangle$  is defined

$$(2.18) \quad |Z\rangle \equiv e^{Z\hat{a}^\dagger} |0\rangle = \sum_n \frac{Z^n}{n!} (\hat{a}^\dagger)^n |0\rangle = \sum_n \frac{Z^n}{\sqrt{n!}} |n\rangle$$

and has the following properties

$$(2.19) \quad \hat{a}|Z\rangle = \sum_n \frac{Z^n}{\sqrt{n!}} \hat{a}|n\rangle = Z \sum_n \frac{Z^{(n-1)}}{\sqrt{(n-1)!}} |n-1\rangle = Z|Z\rangle$$

$$(2.20) \quad \langle Z|Z'\rangle = \sum_{mn} \langle m| \frac{Z^{*m}}{\sqrt{m!}} \frac{Z'^n}{\sqrt{n!}} |n\rangle = e^{Z^*Z'}$$

$$(2.21) \quad \langle Z| : A(\hat{a}^\dagger, \hat{a}) : |Z'\rangle = e^{Z^*Z'} A(Z^*, Z')$$

$$(2.22) \quad \int \frac{dZ dZ^*}{2\pi i} e^{-Z^*Z} |Z\rangle\langle Z| = 1$$

The last relation is most easily demonstrated by writing the complex variable in polar form  $Z = \rho e^{i\phi}$  and performing the  $\phi$  integral first. Analogous results are straightforwardly obtained [8] for a complete set of creation operators  $\hat{a}_\alpha^\dagger$

$$\begin{aligned} |Z\rangle &= e^{\sum_\alpha Z_\alpha \hat{a}_\alpha^\dagger} |0\rangle \\ \hat{a}_\alpha |Z\rangle &= Z_\alpha |Z\rangle \\ \langle Z| : A(\vec{a}^\dagger, \vec{a}) : |Z'\rangle &= e^{\sum_\alpha Z_\alpha Z'_\alpha} A(\vec{Z}^*, \vec{Z}) \\ (2.23) \quad \int \prod_\alpha \frac{dZ_\alpha^* dZ_\alpha}{2\pi i} e^{-\sum_\alpha Z_\alpha^* Z_\alpha} |Z\rangle\langle Z| &\equiv \int d\mu(Z) |Z\rangle\langle Z| = 1 \end{aligned}$$

Proceeding as before, we obtain a path integral by time slicing

$$(2.24) \quad \langle Z_f | e^{-\beta H} | Z_i \rangle = \langle Z_f | e^{-\epsilon H} \int d\mu(Z_n) | Z_n \rangle \langle Z_n | e^{-\epsilon H} \int d\mu(Z_{n-1}) \cdots$$

and the matrix element of the infinitesimal evolution operator is

$$(2.25) \quad \begin{aligned} d\mu(Z_k) \langle Z_k | e^{-\epsilon H} | Z_{k-1} \rangle &= \prod_{\alpha} \frac{dZ_{k\alpha}^* dZ_{k\alpha}}{2\pi i} e^{-\sum_{\alpha} Z_{k\alpha}^* Z_{k\alpha}} \langle Z_k | : e^{-\epsilon H(a^\dagger a)} : + \mathcal{O}(\epsilon^2) | Z_{k-1} \rangle \\ &= \prod_{\alpha} \frac{dZ_{k\alpha}^* dZ_{k\alpha}}{2\pi i} e^{-\sum_{\alpha} Z_{k\alpha}^* (Z_{k\alpha} - Z_{(k-1)\alpha}) - \epsilon H(Z_{k\alpha}^*, Z_{(k-1)\alpha})} \end{aligned}$$

with the result

$$(2.26) \quad \langle Z_f | e^{-\beta H} | Z_i \rangle = \int \mathcal{D}(Z_{k\alpha}^*, Z_{k\alpha}) e^{-S(Z_{k\alpha}^*, Z_{k\alpha})}$$

where

$$(2.27) \quad S(Z^*, Z) = \sum_k \epsilon \left\{ \sum_{\alpha} Z_{k\alpha}^* (Z_{k\alpha} - Z_{(k-1)\alpha}) + H(Z_{k,\alpha}^*, Z_{k-1,\alpha}) \right\}$$

For Fermions with creation and annihilation operators  $c_{\alpha}^{\dagger}$  and  $c_{\alpha}$  one must take an additional step and introduce anticommuting Grassmann variables  $\xi$ , so that if  $\hat{c}_{\alpha}|\xi\rangle = \xi_{\alpha}|\xi\rangle$  and  $\hat{c}_{\beta}|\xi\rangle = \xi_{\beta}|\xi\rangle$ , then we can have  $\hat{c}_{\alpha}\hat{c}_{\beta}|\xi\rangle = \xi_{\alpha}\xi_{\beta}|\xi\rangle = -\xi_{\beta}\xi_{\alpha}|\xi\rangle = -\hat{c}_{\beta}\hat{c}_{\alpha}|\xi\rangle$ . For our present purposes, one may regard this construction as a set of purely formal definitions. Since  $\xi_{\alpha}^2 = 0$ , the only allowable functions are monomials, functions are specified by the non-vanishing terms of their Taylor series, and the definite integral is defined by the properties  $\int d\xi_{\alpha} = 1$  and  $\int d\xi_{\alpha}\xi_{\alpha} = 1$ . Fermion coherent states are then defined by

$$(2.28) \quad |\xi\rangle = e^{-\sum \xi_{\alpha} c_{\alpha}^{\dagger}} |0\rangle$$

and satisfy relations analogous to (2.23) and yield a path integral of the form (2.26). Although there are a few technical details which may be found in Ref.[8], the essential point is that Grassmann coherent states and path integrals have essentially the same form as for Bosons, except for a few crucial minus signs which do all the correct bookkeeping for the difference between Bosons and Fermions.

**2.4. Gaussian Integrals.** – Recall the general formula for the Gaussian integral over complex variables

$$(2.29) \quad \int \prod_i \frac{dx_i^* dx_i}{2\pi i} e^{-x_i^* H_{ij} x_j + J_i^* x_i + J_i x_i^*} = [\det H]^{-1} e^{J_i^* H_{ij}^{-1} J_j}$$

which may be proved by changing to a basis in which  $H$  is diagonal and using  $\int dx e^{-ax^2} = \sqrt{\pi/a}$ . An analogous result is obtained for Grassmann variables by noting that

$$(2.30) \quad \int d\xi^* d\xi e^{-\xi^* a \xi} = \int d\xi^* d\xi (1 - \xi^* a \xi) = a$$



Hence

$$(2.31) \quad \int \prod_i d\xi_i^* d\xi_i e^{-\xi_i^* H_{ij} \xi_j + \eta_i^* \xi_i + \eta_i \xi_i^*} = [\det H] e^{\eta_i^* H_{ij}^{-1} \eta_j}$$

and we see that the only difference between complex variables and Grassmann variables is that  $\det H$  appears to the power  $-1$  and  $1$ , respectively.

With this result, we are prepared to integrate out the Grassmann variables from the path integral. Suppose the action has the form

$$(2.32) \quad S(\xi^*, \xi, \phi) = \xi_i^* M(\phi)_{ij} \xi_j + S_B(\phi)$$

where, for example,  $\xi^*, \xi$  might represent the Fermions  $\bar{\psi}, \psi$  in  $\bar{\psi}(\not{p} - \not{A} + m)\psi + F_{\mu\nu}(A)^2$  and  $\phi$  represents the real Bose field  $A$ . Then

$$(2.33) \quad \int d\xi^* d\xi d\phi e^{\xi^* M(\phi) \xi + S_B(\phi)} = \int d\phi e^{\ln \det M(\phi) + S_B(\phi)}$$

and we are left with an integral over the real field  $\phi$  of an effective action

$$(2.34) \quad S_{\text{eff}}(\phi) = \ln \det M(\phi) + S_B(\phi)$$

In the same way, we can perform the Gaussian integrals for propagators. Consider first the propagator (or contraction in the language of Wick's theorem) corresponding to the thermodynamic average of the time-ordered product of field annihilation and creation operators at space-time points  $i = (x_i t_i)$  and  $j = (x_j t_j)$ , respectively:

$$(2.35) \quad \begin{aligned} \langle T \psi_i \bar{\psi}_j \rangle &= \text{Tr} T \psi_i \bar{\psi}_j e^{-\bar{\psi} M(\hat{\phi}) \psi + S_B(\hat{\phi})} \\ &= \int d\xi^* d\xi d\phi \xi_i \xi_j^* e^{-\xi^* M(\phi) \xi + S_B(\phi)} \\ &= \int d\phi M^{-1}(\phi)_{ij} e^{S_{\text{eff}}(\phi)} \end{aligned}$$

The last line is obtained by differentiating Eq. (2.31) with respect to  $\eta_i$  and  $\eta_j$  which brings down the Grassmann variables  $\xi_i^*$  and  $\xi_j^*$  on the left and the inverse matrix on the right. The general integral with  $n$  pairs of creation and annihilation operators follows similarly from taking  $n$  pairs of derivatives and yields the general form of Wick's theorem:

$$(2.36) \quad \begin{aligned} &\int \mathcal{D}(\xi^* \xi) \xi_{i_1} \cdots \xi_{i_n} \xi_{j_n}^* \cdots \xi_{j_1}^* e^{-\xi^* M \xi} \\ &= \frac{\delta^{2n}}{\delta \eta_{i_1}^* \cdots \delta \eta_{i_n}^* \delta \eta_{j_n} \cdots \delta \eta_{j_1}} \int \mathcal{D}(\xi^* \xi) e^{-\xi_i^* M_{ij} \xi_j + \eta_i^* \xi_i + \eta_i \xi_i^*} \Big|_{\eta = \eta^* = 0} \\ &= \frac{\delta^{2n}}{\delta \eta_{i_1}^* \cdots \delta \eta_{i_n}^* \delta \eta_{j_n} \cdots \delta \eta_{j_1}} \det H e^{\eta_i^* M_{ij} \eta_j} \Big|_{\eta = \eta^* = 0} \\ &= \sum_P (-1)^P M_{i_P n j_n}^{-1} \cdots M_{i_P 1 j_1}^{-1} e^{\ln \det H} \end{aligned}$$

where  $P$  denotes a permutation of the  $n$  indices. Hence, the Fermions may be integrated out of any physical observable when the action has the form (2.32), leaving the sum of all possible contractions weighted by the effective action (2.34), and we are left with an effective theory containing only Bosonic degrees of freedom.

### 3. – Lattice QCD for Gluons

It is useful to begin the study of lattice gauge theory with the simplest possible gauge theory, and gradually increase the generality and complexity one step at a time. Hence, in this section we will completely ignore Fermions, and concentrate only on the pure gluon sector. This will correspond to the physical limit in which the quark mass goes to infinity and quarks cease to be dynamical degrees of freedom. Furthermore, we will begin with the simplest possible gauge group,  $U(1)$  corresponding to QED, and only after motivating and displaying the Wilson action for this case will we move to the non-Abelian  $SU(N)$  gauge theory.

**3.1.  $U(1)$  Gauge Theory and the Wilson Action.** – To motivate the way gauge theory will be formulated on a discrete space-time lattice, it is useful to recall the essential ideas underlying continuum gauge theory, and how the entire theory may be viewed as arising from the principle of gauge invariance. Therefore, let us consider a Lagrangian for a complex scalar field

$$(3.1) \quad L = \partial_\mu \phi^* \partial_\mu \phi - V(\phi^* \phi)$$

and look for the simplest extension of the theory which is consistent with local gauge invariance. Note that since our final goal will be to calculate Euclidean path integrals, we will always write the Lagrangian and action in Euclidean form, with the result that  $g_{\mu\nu} = \delta_{\mu\nu}$  and upper and lower Dirac indices are equivalent. Whereas  $L$  is manifestly invariant under the global gauge transformation  $\tilde{\phi}(x) = -e^{-i\alpha} \phi(x)$ , the derivatives in  $L$  yield new terms in the case of a local transformation  $\tilde{\phi}(x) = e^{-i\alpha(x)} \phi(x)$

$$(3.2) \quad \partial_\mu \tilde{\phi}^* \partial_\mu \tilde{\phi} = [(\partial_\mu - i(\partial_\mu \alpha)) \phi]^* (\partial_\mu - i(\partial_\mu \alpha)) \phi$$

If we adopt the principle of local gauge invariance, that the theory should be independent of the arbitrary phase choice  $\alpha(x)$  that various observers might choose at different points in space, then we may repair the theory by adding a “compensating” field  $A_\mu(x)$  such that

$$(3.3) \quad \tilde{A}_\mu(x) = A_\mu(x) + \frac{1}{g} \partial_\mu \alpha(x)$$

If we now replace the derivative  $\partial_\mu$  in  $L$  by the covariant derivative

$$(3.4) \quad D_\mu \phi(x) \equiv (\partial_\mu + igA_\mu(x)) \phi(x)$$

we observe that the transformation of  $A_\mu(x)$  exactly compensates for the undesired derivative of  $\alpha$  and yields an invariant Lagrangian.

Whereas the coupling of the new field  $A$  to  $\phi$  was determined from gauge invariance, the only guiding principle for determining the action for  $A$  itself is simplicity and economy. Thus, we seek the simplest action for  $A_\mu$  involving the least number of derivatives which is consistent with gauge invariance and Lorentz invariance. Noting that

$$(3.5) \quad \partial_\mu \left( A_\nu + \frac{1}{g} \partial_\nu \alpha \right) - \partial_\nu \left( A_\mu + \frac{1}{g} \partial_\mu \alpha \right) = \partial_\mu A_\nu - \partial_\nu A_\mu \equiv F_{\mu\nu}$$

we observe that  $F_{\mu\nu}$  is gauge invariant so that  $F_{\mu\nu}^2$  is both gauge and Lorentz invariant and we are thus led automatically to Maxwell's equations and the complete Lagrangian

$$(3.6) \quad L = -\frac{1}{4e^2} (\partial_\mu A_\nu - \partial_\nu A_\mu)^2 + (D_\mu \phi)^* (D_\mu \phi) - V(\phi^* \phi) \quad .$$

For subsequent treatment on a lattice, it is useful to note that the appropriate operator to compare fields at two different points  $x$  and  $y$  is the link variable

$$(3.7) \quad U(y, x) = e^{i \int_x^y dx_\mu g A_\mu(x)}$$

which simply removes the arbitrary phases between the two points and yields a gauge invariant result.

We now consider how to approximate this continuum theory on a space-time lattice. Often in numerical analysis, one may allow discrete approximations to break fundamental underlying symmetries. For example, when one solves the time-independent Schrödinger equation on a spatial mesh, one violates translational invariance. There may be small spurious pinning forces which reflect the fact that the energy is slightly lower when the solution is centered on a mesh site or centered between mesh sites, but there are no major qualitative errors and the quantitative errors may be strictly controlled. When one solves the time-dependent Schrödinger equation or time-dependent Hartree-Fock equation, however, one finds that it is important to enforce certain properties such as energy conservation and unitarity when discretizing the problem in time. In the case of lattice gauge theory, since by the previous argument gauge invariance plays such a crucial role in defining the theory, it is desirable to enforce it exactly in the lattice action. In contrast, as in the case of the Schrödinger equation, we will settle for an action which breaks Lorentz invariance, and simply insist on making the lattice spacing small enough that the errors are acceptably small.

Following Wilson, we define the action in terms of directed link variables assigned to each of the links between sites of the space-time lattice. For  $U(1)$ , we define the link variable from site  $n$  in the  $\mu$  direction to site  $n + \mu$  as a discrete approximation to the integral  $e^{ig \int_n^{n+\mu} dx A_\mu}$  which we denote

$$(3.8) \quad U_\mu(n) = e^{i\theta_\mu(n)} = e^{iagA_\mu(n+\frac{\mu}{2})} \quad .$$

Thus  $\theta_\mu(n)$  is a discrete approximation to  $g \int_n^{n+\mu} dx A_\mu$  along the direction of the link, with  $A_\mu$  evaluated at the center of the link. When the direction is reversed,  $U_n(n) \rightarrow$

$U_n(n)^\dagger$ . The link variable is then a group element of  $U(1)$  and the compact variable  $\theta_\mu(n)$  will be associated with  $agA_\mu(x)$  in the continuum limit. With these link variables, the integral over the field variables in the path integral is replaced by the invariant group measure for  $U(1)$ , which is  $\frac{1}{2\pi} \int_{-\pi}^{\pi} d\theta$ .

The fundamental building blocks of the lattice action are products of directed link variables taken counter-clockwise around each individual plaquette of the lattice. By construction, this product is gauge invariant, ensuring gauge invariance of the resulting action. A typical plaquette is sketched in Fig. 1,  $\mu$  and  $\nu$  are unit vectors in the horizontal and vertical directions, the position of the center of the plaquette is  $x$ , and we express the centers of each link in terms of displacements  $\pm\frac{a}{2}$  in the  $\mu$  or  $\nu$  directions. The product of the four group elements around the plaquette may thus be written

$$\begin{aligned}
U_{\mu\nu}^\square &= \prod_{\square} U_1 U_2 U_3^\dagger U_4^\dagger \\
&= e^{ia g [A_\mu(x - \frac{a}{2}\nu) + A_\nu(x + \frac{a}{2}\mu) - A_\mu(x + \frac{a}{2}\nu) - A_\nu(x - \frac{a}{2}\mu)]} \\
&\cong e^{ia^2 g (\partial_\mu A_\nu - \partial_\nu A_\mu)} \\
(3.9) \quad &= e^{ia^2 g F_{\mu\nu}} \quad .
\end{aligned}$$

Note that the discrete lattice difference operator  $A_\nu(x + \frac{a}{2}\mu) - A_\nu(x - \frac{a}{2}\mu)$  becomes the derivative  $a\partial_\mu A_\nu$  in the continuum limit, so that the exponent is a discrete approximation to the curl on the lattice and is proportional to  $\partial_\mu A_\nu - \partial_\nu A_\mu = F_{\mu\nu}$  in the continuum. Since each plaquette generates an approximation to  $F_{\mu\nu}$ , an action which corresponds to QED in the continuum limit may be constructed by choosing a function of  $U_{\mu\nu}^\square$  which yields  $F_{\mu\nu}^2$  plus terms that are negligible in the continuum limit. Defining the inverse coupling constant  $\beta_g = 1/g^2$ , where the subscript  $g$  distinguishes it from other quantities commonly denoted by  $\beta$ , and expanding in the limit  $a \rightarrow 0$ , the action may be written

$$\begin{aligned}
S(U) &= \beta_g \sum_{\square} (1 - \text{Re } U^\square) \\
&\sim \frac{1}{g^2} \sum_{\square} (1 - \cos(a^2 g F_{\mu\nu})) \\
&\sim \frac{1}{g^2} \sum_{n\{\mu\nu\}} \left( \frac{a^4 g^2}{2} F_{\mu\nu}^2(n) + \dots \right) \\
&\sim \frac{1}{2} \sum_n a^4 \sum_{\{\mu\nu\}} F_{\mu\nu}^2(n) \\
(3.10) \quad &\rightarrow \frac{1}{4} \int d^4x F_{\mu\nu}(x) F_{\mu\nu}(x) \quad .
\end{aligned}$$

In the second line  $\{\mu\nu\}$  denotes the sum over all pairs of  $\mu$  and  $\nu$  arising from the sum over plaquettes and the extra factor of  $1/2$  in the last line accounts for the fact that each pair occurs twice in the double sum over repeated indices  $F_{\mu\nu}F_{\mu\nu}$ . The terms higher order in the lattice cutoff  $a$  vanish in the classical continuum limit and may give rise to

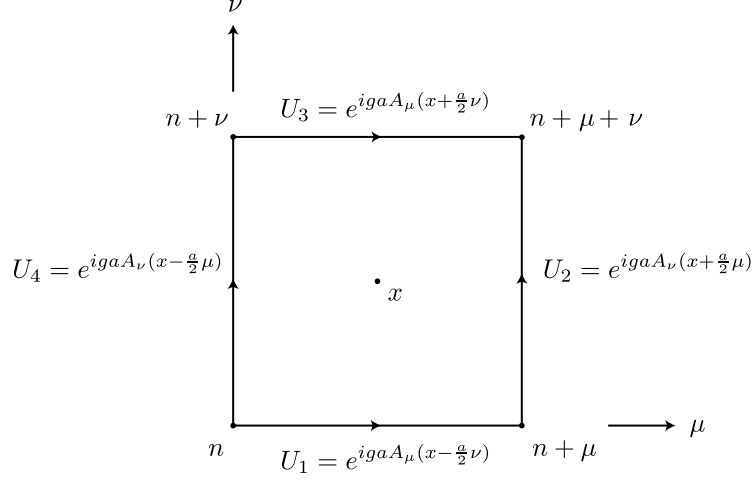


Fig. 1. – An elementary plaquette of link variables.

finite renormalization of the coupling constant in quantum field theory. The lattice gauge theory defined by (3.10) is in a form which may be solved directly using the Metropolis or heat bath methods. For readers worried that we have not systematically accounted for all corrections of higher order in  $a$ , a more complete derivation will be presented later for the general  $SU(N)$  case.

It is useful to examine the role of Gauss' law and how the presence of external charges is manifested in this theory. The basic ideas are most easily sketched in the continuum theory. Since the Hamiltonian does not constrain the charge state of the system, we must project the states appearing in the path integral onto the space satisfying  $\vec{\nabla} \cdot \vec{E} = \rho$  with a specific background charge  $\rho$ , which may be accomplished by writing a  $\delta$ -function in the form  $\int \mathcal{D}\chi e^{i \int dx dt \chi (\vec{\nabla} \cdot \vec{E} - \rho)}$ . Remaining in temporal gauge  $A_0 = 0$  and using the form of the path integral (2.2) in which both the coordinate  $x \rightarrow A$  and momentum  $\rho \rightarrow E$  appear, the path integral for the partition function projected onto the space with external source  $\rho$  may be written

$$\begin{aligned}
 (3.11) \quad Z &= \int \mathcal{D}\chi \mathcal{D}\vec{A} \mathcal{D}\vec{E} e^{\int dx dt [i\vec{E} \cdot \dot{\vec{A}} - \frac{1}{2}(E^2 + B^2) + i\chi(\vec{\nabla} \cdot \vec{E} - \rho)]} \\
 &= \int \mathcal{D}\chi \mathcal{D}\vec{A} e^{-\int dx dt \left\{ \frac{1}{2} [(\dot{\vec{A}} - \vec{\nabla}\chi)^2 + B^2 - i\chi\rho] \right\}} .
 \end{aligned}$$

Equation (3.11) is an important result. Having started in temporal gauge  $A_0 = 0$ , we see that enforcing Gauss' law gives rise to a projection integral over an additional field  $\chi$  which enters into the final action just like the original  $A_0$  field. Indeed, renaming  $\chi = A_0$  so that  $\dot{A}_i - \partial_i A_0 = F_{0i}$  and writing the source as a set of point charges

$\rho(x) = \sum_n q_n \delta(x - x_n)$ , we obtain

$$(3.12) \quad Z = \int \mathcal{D}A_\mu e^{-\int dx dt \frac{1}{4} F_{\mu\nu} F_{\mu\nu}} \prod_n e^{-iq_n \int dt A_0(x_n, t)} .$$

Thus, the Hamiltonian path integral with projection is precisely the Lagrangian path integral with a line of  $\pm A_0$  fields at the positions of the fixed external  $\pm$  charges. In the case of no external charges, we may think of the Lagrangian path integral including the  $A_0$  integral as the usual filter  $e^{-\beta H}$  selecting out the ground state. In the presence of charges, the path integral augmented by lines of  $A_0$  at the positions of the charges filters out the ground state in the presence of these sources.

**3.2.  $SU(N)$  Gauge Theory.** – The generalization to non-Abelian gauge theory is straightforward. The link variables become group elements of  $SU(N)$

$$(3.13) \quad U_\mu(n) = e^{iag\frac{1}{2}\lambda^c A_\mu^c(n)} \equiv e^{iag\tilde{A}_\mu(n)}$$

where the  $\lambda^c$  are Pauli matrices or Gell–Mann matrices for  $SU(2)$  or  $SU(3)$  and  $c$  is a color label which runs over the  $N^2 - 1$  generators  $\lambda^c$ . The integration in the path integral is defined by the invariant group measure which we will denote by  $\mathcal{D}(U)$ .

Since derivation of the  $SU(N)$  action is one of our primary results, let us be slightly more careful than in the  $U(N)$  case and keep track of higher order terms in  $a$  to ascertain the leading error in our result.[13] As before, we refer the centers of each of the links in Fig. 1 to the point  $x$  in the center of the plaquette, so that for  $SU(N)$

$$(3.14) \quad \begin{aligned} U_1 &= e^{iga\tilde{A}_\mu(x - \frac{a}{2}\nu)} & U_2 &= e^{iga\tilde{A}_\nu(x + \frac{a}{2}\mu)} \\ U_3 &= e^{iga\tilde{A}_\mu(x + \frac{a}{2}\nu)} & U_4 &= e^{iga\tilde{A}_\nu(x - \frac{a}{2}\mu)} \end{aligned}$$

and the product of  $SU(N)$  group elements around an elementary plaquette is

$$(3.15) \quad U_{\mu\nu}^\square = \prod_{\square} U_1 U_2 U_3^\dagger U_4^\dagger$$

With this notation, we note that  $U_1(-a) = U_3^\dagger(a)$  and  $U_2(-a) = U_4^\dagger(a)$ . Hence,  $\text{Tr} U_{\mu\nu}^\square(-a) = \text{Tr} U_3^\dagger U_4^\dagger U_1 U_2 = \text{Tr} U_{\mu\nu}^\square(a)$  so that  $\text{Tr} U_{\mu\nu}^\square$  is an even function of  $a$ . Also, because  $U_{\mu\nu}^\square$  is a product of unitarity matrices,  $U_{\mu\nu}^\square U_{\mu\nu}^{\square\dagger} = 1$ . The continuum contribution is obtained by expanding  $\tilde{A}_\mu(x - \frac{a}{2}\nu) = \tilde{A}_\mu(x) - \frac{a}{2} \frac{\partial}{\partial \nu} \tilde{A}_\mu + \theta(a^2)$  as before and applying the Baker–Hausdorff identity  $e^{\hat{x}} e^{\hat{y}} = e^{(\hat{x}\hat{y} + \frac{1}{2}[\hat{x}\hat{y}] + \dots)}$  to each quantity below in curly brackets, with the result

$$(3.16) \quad \begin{aligned} U_{\mu\nu}^\square &= \left\{ e^{iag(A_\mu - \frac{a}{2}\partial_\nu A_\mu + \mathcal{O}(a^2))} e^{ig(A_\nu + \frac{a}{2}\partial_\mu A_\nu + \mathcal{O}(a^2))} \right\} \\ &\quad \times \left\{ e^{iag(A_\mu + \frac{a}{2}\partial_\nu A_\mu + \mathcal{O}(a^2))} e^{ig(A_\nu - \frac{a}{2}\partial_\mu A_\nu + \mathcal{O}(a^2))} \right\} \\ &= e^{iag(A_\mu + A_\nu + \frac{a}{2}(\partial_\mu A_\nu - \partial_\nu A_\mu) + \frac{iaa}{2}[A_\mu, A_\nu] + \mathcal{O}(a^2))} \\ &\quad \times e^{iag(-A_\mu - A_\nu + \frac{a}{2}(\partial_\mu A_\nu - \partial_\nu A_\mu) + \frac{iaa}{2}[A_\mu, A_\nu] + \mathcal{O}(a^2))} \\ &= e^{iag[a(\partial_\mu A_\nu - \partial_\nu A_\mu) + iag[A_\mu, A_\nu] + \mathcal{O}(a^2)]} \end{aligned}$$

Writing  $F_{\mu\nu} \equiv \partial_\mu A_\nu - \partial_\nu A_\mu + ia g [A_\mu, A_\nu]$  and defining the next two terms in an expansion in powers of  $a$  as  $G_{\mu\nu}$  and  $H_{\mu\nu}$ , we obtain

$$(3.17) \quad \begin{aligned} U_{\mu\nu}^\square &= e^{ia^2 g F_{\mu\nu} + ia^3 G_{\mu\nu} + ia^4 H_{\mu\nu}} \\ &= 1 + ia^2 F_{\mu\nu} + ia^3 G_{\mu\nu} + ia^4 H_{\mu\nu} - \frac{a^4}{2} g^2 F_{\mu\nu}^2 + \theta(a^5) \end{aligned}$$

Unitarity of  $U_{\mu\nu}^\square$  implies that  $F$ ,  $G$  and  $H$  are Hermitian which combined with the fact that  $\text{Tr} U_{\mu\nu}^\square$  is an even function of  $a$  yields

$$(3.18) \quad \text{Re Tr} U_{\mu\nu}^\square = \frac{1}{2} \text{Tr}(U_{\mu\nu}^\square + U_{\mu\nu}^{\square\dagger}) = \text{Tr}(1 - \frac{1}{2} a^4 g^2 F_{\mu\nu}^2) + \theta(a^6)$$

Defining the inverse coupling  $\beta_g = 2N/g^2$ , the  $SU(N)$  action may be written

$$(3.19) \quad \begin{aligned} S(U) &= \beta_g \sum_{\square} \left( 1 - \frac{1}{N} \text{Re Tr} U_{\square} \right) \\ &= \frac{\beta_g a^4 g^2}{2N} \sum_{n\{\mu\nu\}} \text{Tr} \left( \frac{1}{2} \lambda^c F_{\mu\nu}^c \frac{1}{2} \lambda^b F_{\mu\nu}^b \right) + \mathcal{O}(a^6) \\ &= \sum_n a^4 \sum_{\{\mu\nu\}} \frac{1}{2} F_{\mu\nu}^c(n) F_{\mu\nu}^c(n) + \mathcal{O}(a^6) \\ &\rightarrow \frac{1}{4} \int d^4x F_{\mu\nu}^c(x) F_{\mu\nu}^c(x) + \mathcal{O}(a^6) . \end{aligned}$$

Note that summation over repeated indices is implied everywhere except where  $\sum_{\{\mu\nu\}}$  denotes sums over distinct pairs, and the property  $\text{Tr} \lambda^b \lambda^c = 2\delta_{bc}$  has been used in the second line.

**3.3. Wilson Loops and Lines.** – Rephrasing the original discussion of gauge fields in terms of lattice variables, if there were a quark field defined on a lattice, then under a local gauge transformation, the field  $\psi_i$  at each site would be multiplied by a group element  $g_i$ . The link variables were explicitly introduced to compensate such a gauge transformation, so the link variable  $U_{ij}$  going from site  $i$  to  $j$  is multiplied by  $g_i$  and  $g_j^{-1}$ . Thus, the overall effect of a gauge transformation is the following:

$$(3.20) \quad \begin{aligned} U_{ij} &\rightarrow g_i U_{ij} g_j^{-1} \\ \psi_i &\rightarrow g_i \psi_i \\ \bar{\psi}_i &\rightarrow \bar{\psi}_i g_i^{-1} . \end{aligned}$$

In the pure gauge sector, where the only variables are link variables, it is clear from (3.20) that the only gauge invariant objects which can be constructed are products of link variables around closed paths, for which the factors of  $g$  and  $g^{-1}$  combine at each site. The Wilson loop is therefore defined as the trace of a closed loop of link variables

$$(3.21) \quad \begin{aligned} W &\equiv \text{Tr} \prod_{ij \in c} U_{ij} \\ &= \text{Tr} U_{ij} U_{jk} \cdots U_{mn} U_{ni} \end{aligned}$$

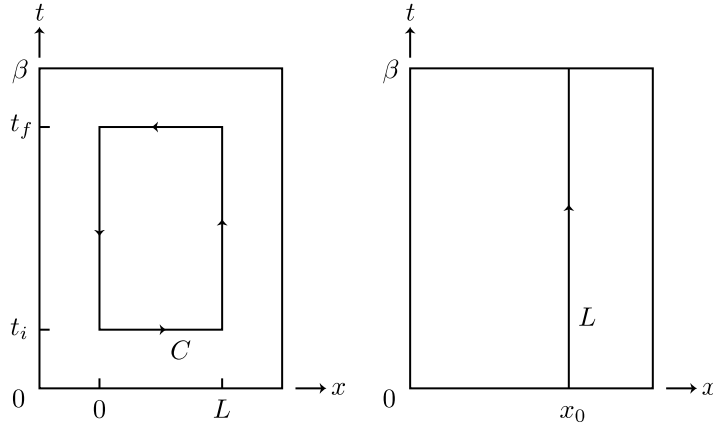


Fig. 2. – A space-time Wilson loop defined by the chain of link variables  $C$  on a finite lattice (left) and a Wilson or Polyakov line defined by the chain of link variables  $L$  on a finite lattice (right).

and specifies the rotation in color space that a quark would accumulate along the loop  $c$  from the path-ordered product  $P_c e^{\int ig\bar{A}}$ .

To understand the physical significance of a space-time Wilson loop, it is useful to note that by (3.20), a quark creation operator at site  $j$  and an annihilation operator at site  $i$  transform under gauge transformations like a product of link variables connecting sites  $i$  and  $j$

$$(3.22) \quad \begin{aligned} \psi_i \bar{\psi}_j &\rightarrow g_i \psi_i \bar{\psi}_j g_j^{-1} \\ U_{ik} U_{k\ell} \cdots U_{mj} &\rightarrow g_i U_{ik} U_{k\ell} \cdots U_{mj} g_j^{-1} . \end{aligned}$$

Thus, as far as the gluon fields are concerned, the ends of a chain of link variables are equivalent to an external quark-antiquark source, and the presence of such a chain of link variables therefore measures the response of the gluon fields to an external quark-antiquark source.

Now, consider the time evolution of the system corresponding to the expectation value of the Wilson loop drawn in Figure 2

$$(3.23) \quad \langle W \rangle = \frac{\int dU e^{-S(U)} \text{Tr} \prod_C U_{ij}}{\int dU e^{-S(U)}} .$$

Prior to the time  $t_i$ , there are no color sources present, so evolution filters out the gluon ground state in the zero charge sector,  $|0\rangle = e^{-t_i H} |Q=0\rangle$ . At time  $t_i$ , the line of link variables between 0 and  $L$  creates an external antiquark source at 0 and a quark source at  $L$ . As discussed in connection with Eq. (3.12), the links in the time direction between  $t_i$  and  $t_f$  maintain these sources at 0 and  $L$ . Hence, for any  $t$  between  $t_i$  and  $t_f$ , the



evolution filters out the lowest gluon configuration in the presence of external quark-antiquark sources producing the state  $|\psi\rangle = e^{-(t-t_i)H}\psi(0)\bar{\psi}(L)|0\rangle$ . Finally, at time  $t_f$ , the external sources at 0 and  $L$  are removed by a line of links from  $L$  to 0, and the system is returned to the zero charge sector. Using Feynman's picturesque language of antiquarks corresponding to quarks propagating backwards in time, one may succinctly characterize the Wilson loop as measuring the response of the gluon fields to an external quark-like source traveling around the perimeter of the space-time loop in the direction of the arrows.

Quantitatively, if  $t_f - t_i$  is large enough, the lowest gluon state in the presence of quark and antiquark sources separated by  $L$  will dominate, and  $\langle W \rangle$  will be proportional to  $e^{-(t_f-t_i)V(L)}$  where  $V(L)$  is the static quark-antiquark potential. Physically, this potential corresponds to the potential arising in heavy quark spectroscopy. Furthermore, at large distances, the potential in the pure gluon sector becomes linear (since the flux tube cannot be broken by  $q\bar{q}$  pair creation) so the Wilson loop enables direct numerical calculation of the string tension. If the Wilson loop has  $I$  links in the time direction and  $J$  links in the space direction, then

$$(3.24) \quad W(IJ) = \left\langle \text{Tr} \prod_{C_{IJ}} U \right\rangle \underset{I \rightarrow \infty}{\sim} e^{-aIV(aJ)} \underset{I, J \rightarrow \infty}{\sim} e^{-a^2 \sigma IJ} .$$

The exponent is thus proportional to the area for large loops, and this area behavior is a signature of confinement, since it arises directly from the linearly rising potential. Although the preceding physical argument was framed in Hamiltonian form with evolution in the time direction, it is clear that because of the symmetry of the Euclidean action, all space-time dimensions are equivalent and the area law reflects this symmetry.

Since the string tension can be calculated directly from Wilson loops, it is useful to relate it to an experimentally measurable quantity, the slope of Regge trajectories. It is an empirical fact that families of meson states with a given set of internal quantum numbers have mass dependence on the total angular momentum  $J$  which is accurately described by the Regge formula

$$(3.25) \quad M_J^2 = \frac{1}{\alpha'} J \quad , \quad \alpha' = 0.9 \text{ GeV}^{-2} \quad .$$

To see how the slope  $\alpha'$  is related to the string tension, it is useful to consider a very simple model in which a massless quark and antiquark are connected by a string or flux tube of length  $2L$ . Since the quarks are massless, they must move at the speed of light, and the velocity of the segment of string a distance  $x$  from the origin is  $v = \frac{x}{L}$ . If  $\sigma$  is defined as the energy per unit length of the flux tube in its rest frame, then the contributions of the element of length  $dx$  at point  $x$  to the energy and angular momentum are

$$(3.26) \quad dE = \gamma \sigma dx \quad , \quad dJ = \gamma \sigma v x dx$$

where  $v = \frac{x}{L}$  (with  $c = 1$ ) and  $\gamma = (1 - v^2)^{-1/2}$ . Hence,

$$(3.27) \quad M = \int_{-L}^L \frac{\sigma dx}{\sqrt{1 - (\frac{x}{L})^2}} = \pi\sigma L \quad , \quad J = \int_{-L}^L \frac{\sigma \frac{x^2}{L} dx}{\sqrt{1 - (\frac{x}{L})^2}} = \frac{\pi}{2}\sigma L^2$$

and

$$(3.28) \quad M^2 = \pi^2 \sigma^2 L^2 = 2\pi\sigma J$$

so that

$$(3.29) \quad \sqrt{\sigma} = [2\pi\alpha']^{-1/2} = 420 \text{ MeV} \quad .$$

Clearly this flux tube model is a drastic oversimplification, especially for low angular momentum states for which the finite width of the tube, the structure of the end caps, and the lack of localization of the quarks could all produce large corrections. At large angular momentum, however, the picture is somewhat more convincing. In the context of this model, I will therefore take the point of view that the accurate Regge behavior at low angular momentum is accidental and that  $\sigma$  is primarily determined by high angular momentum states. However, since the ultimate theory is undoubtedly much more complicated, I will not regard it as a serious problem if lattice parameters determined from this rough argument disagree at the 5 to 10% level relative to those determined from other observables such as direct calculation of hadron masses.

Although the area law behavior of large Wilson loops is clear from (3.24), in practical calculations on finite lattices, there are significant corrections, including a term proportional to the perimeter arising from the self-energy of the external sources and a constant arising from gluon exchanges at the corners, so that

$$(3.30) \quad -\ln W(I, J) \sim C + D(I + J) + a^2\sigma IJ \quad .$$

To eliminate the constant and perimeter terms, the following ratio introduced by Creutz [9] of Wilson loops having the same perimeter is calculated to cancel out the  $C$  and  $D$  terms in (3.30)

$$(3.31) \quad \chi(I, J) = -\ln \left( \frac{W(I, J)W(I-1, J-1)}{W(I, J-1)W(I-1, J)} \right) \sim a^2\sigma \quad .$$

A Wilson or Polyakov line is another form of gauge invariant closed loop which can be placed on a periodic lattice. In this case, as sketched in Fig. 2, the links are located at a fixed position in space  $x_0$  and run in the time direction from the first time slice to the last, which by periodicity is equivalent to the first and thus renders the product gauge invariant. If the length of the lattice in the time direction is  $\beta_t$  (were the subscript  $t$  distinguishes it from the inverse coupling constant  $\beta_g \equiv \frac{2N}{g^2}$ ), the expectation value of the Wilson line yields the partition function for the gluon field in the presence of a single

fixed quark at inverse temperature  $\beta_t$  and thus specifies the free energy  $F_{\text{quark}}$  of a single quark

$$\begin{aligned} \langle \hat{L} \rangle &= \frac{\int \mathcal{D}U e^{-S(U)} \text{Tr} \prod_L U_{ij}}{\int \mathcal{D}U e^{-S(U)}} \\ (3.32) \qquad &= e^{-\beta_t F_{\text{quark}}} \end{aligned}$$

This quantity is useful as an order parameter for the deconfinement phase transition. Note that because the periodic lattice is a four-dimensional torus and  $L$  winds around the lattice once in the time direction, it is characterized by a winding number and is thus topologically distinct from a Wilson loop which has winding number 0. By the preceding argument, two lines in opposite directions, one at  $x = 0$  and one at  $x = L$ , will produce the free energy of a quark and antiquark separated by distance  $L$ , and as  $\beta_t \rightarrow \infty$  this provides a means of calculating the average of the singlet and octet static quark-antiquark potentials.

**3.4. Strong Coupling Expansion.** – One can obtain a useful physical picture of what happens when one evaluates the expectation value of a Wilson loop

$$(3.33) \qquad \langle W \rangle = Z^{-1} \int \mathcal{D}(U) e^{-\beta_g \sum_{\square} (1 - \frac{1}{2N} \text{tr}(U_{\square} + U_{\square}^{\dagger}))} \text{tr} \prod_C U$$

by expanding the exponent in powers of the inverse coupling constant  $\beta_g \equiv \frac{2N}{g^2}$ . Since this expansion requires small  $\beta_g$  and thus large  $g^2$ , it is called the strong coupling expansion. Note that although it is formally analogous to the high temperature expansion in statistical mechanics, where  $\beta_g$  would be replaced by the inverse temperature, the actual physical temperature of our system is specified by the length of the lattice in the time direction,  $\beta_t$ , and is distinct from  $\beta_g$ .

The structure of the expansion is revealed by considering the integrals over group elements which arise in the path integral (3.33). A general discussion of integration over  $SU(N)$  group elements is given by Creutz [9], but for our present purposes it is sufficient to use the following two results, where Greek indices denote  $SU(N)$  matrix indices, not sites

$$(3.34) \qquad \int dU U_{\alpha\beta} = 0$$

$$(3.35) \qquad \int dU U_{\alpha\beta} U_{\gamma\delta}^{-1} = \frac{1}{N} \delta_{\alpha\delta} \delta_{\beta\gamma}$$

These results follow directly from the orthogonality relation for irreducible matrix representations of the group and are trivially verified for  $U(1)$  for which the invariant measure is  $\int dU = \frac{1}{2\pi} \int_{-\pi}^{\pi} d\theta$  and  $U = e^{i\theta}$ .

Now consider the diagrams which result from drawing the links in the Wilson loop  $\prod_C U$  and some set of plaquettes  $U_{\square}$  and  $U_{\square}^{\dagger}$  obtained from expanding the exponential in (3.33). The integral (3.34) tells us that any diagram which has a single exposed link (that

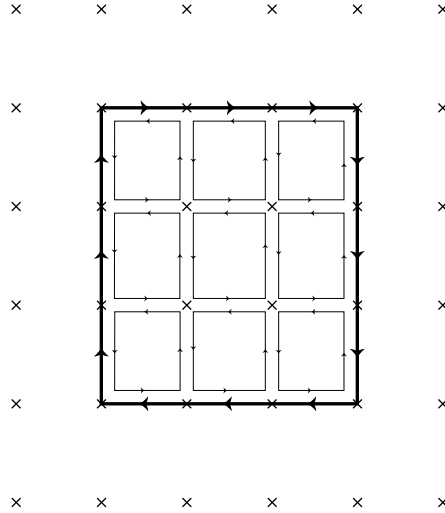


Fig. 3. – A  $3 \times 3$  Wilson loop tiled with plaquettes in the strong coupling expansion.

is, a single link between a pair of sites) anywhere on the lattice gives no contribution. Thus, the only non-vanishing terms in the expansion are those in which we manage to mate plaquettes from the exponential with the Wilson loop to eliminate all exposed links. The simplest way to mate two links to obtain a non-vanishing result is to place them between the same sites in opposite directions, which by (3.35) yields  $\frac{1}{N}$ . Since each plaquette brings with it a factor of  $\beta$ , the lowest order non-vanishing contribution to  $\langle W \rangle$  is obtained by “tiling” the interior of the Wilson loop with plaquettes oriented in the opposite direction as sketched in Fig. 3 for a  $3 \times 3$  loop. Note that each of the outer links of the original Wilson loop is protected, and the interior links protect each other pairwise. The leading term for an  $I \times J$  Wilson loop would thus have  $I \times J$  tiles, each contributing a factor  $\frac{\beta}{2N}$ . In addition, because of the traces in the plaquettes and Wilson loop in (3.33) and the  $\delta$ 's in Eq. (3.35) there is a factor of  $N$  for each of the  $(I+1)(J+1)$  sites and because of the factor  $\frac{1}{N}$  in (3.35) there is a factor  $\frac{1}{N}$  for each of the  $(2IJ+I+J)$  double bonds. Hence, except for  $SU(2)$ , where the counting is different because the two orientations of plaquettes are equivalent, the overall contribution goes as

$$(3.36) \quad W(IJ) \sim \left( \frac{\beta}{2N^2} \right)^{IJ}$$

giving the lowest order contribution to the string tension

$$(3.37) \quad \sigma \sim -a^{-2} \ln \left( \frac{\beta}{2N^2} \right) .$$

Fancier tilings are also possible if one is willing to use more tiles and thus include more powers of  $\beta$ . For example, one could place five tiles together to make a cubic box with an open bottom and replace one or more tiles with this box. The box could be elongated,

or even grown into a tube which connects back somewhere else. Alternatively, one could replace a plaquette oriented in one direction by  $(N-1)$  plaquettes oriented in the opposite direction to obtain a non-vanishing  $SU(N)$  integral.

The utility of this expansion is twofold. It provides a physical picture of filling in the Wilson loop with a gluon membrane, whose vibrations and contortions represent all the quantum fluctuations of the gluon field. When observed on a particular time slice, the cross section of this surface corresponds to a color flux tube joining the quark-antiquark sources. In addition, in low orders, the individual terms can be calculated explicitly and provide a valuable quantitative check of numerical calculations.

**3.5. Continuum Limit and Renormalization.** – Pure gauge theory on a finite lattice is specified by two parameters: the dimensionless bare coupling constant  $g$  and the lattice spacing  $a$  corresponding to a momentum cutoff  $p_{\max} \sim \frac{\pi}{a}$ . As  $a$  is changed, the bare  $g$  must be changed to keep physical quantities fixed.

In principle, the renormalization procedure on a lattice is very simple and could be carried out as follows. First, pick an initial value of  $g$  and calculate some set of dimensionful physical observables  $\langle \mathcal{O}_i \rangle$ . These observables may be written in the form

$$(3.38) \quad \langle \mathcal{O}_i \rangle = a^{-d_i} \langle f_i(g) \rangle$$

where  $d_i$  is the dimension of the operator and  $f_i$  is the dimensionless quantity calculated on the lattice using the Wilson action with  $\beta = \frac{2N}{g^2}$  and with all lengths expressed in units of the lattice spacing  $a$ . For example, we have already seen in Eq. (3.31) that the string tension has the form  $\sigma = a^{-2}\chi$ . Then, use the physical value of one operator, say  $\mathcal{O}_1$ , to determine the physical value of  $a$  corresponding to the selected  $g$ . Again, using the string tension example, we could define  $a = \sqrt{\chi}/420 \text{ MeV}$ . With this value of  $a$  determined from  $\mathcal{O}_1$ , all other observables  $\mathcal{O}_2 \cdots \mathcal{O}_N$  are completely specified. One should then repeat this procedure for a sequence of successively smaller and smaller values of  $g$ , thereby determining the function  $a(g)$  and a sequence of values for the observables  $\mathcal{O}_2 \cdots \mathcal{O}_N$ . If the theory is correct, then each sequence of observables  $\mathcal{O}_i$   $i \neq 1$  should approach a limit as  $g \rightarrow 0$ , and that limit should agree with nature.

In practice, it would be very difficult to carry out a series of calculations as described above to small enough  $g$  to make a convincing case. Hence, it is preferable to make use of our knowledge of the relation between the coupling constant and cutoff based on the renormalization group in the perturbative regime, and only carry out explicit lattice calculations down to the point at which the renormalization group behavior is clearly established. The foundation of the argument is the fact that the first two coefficients in the expansion of the renormalization group function  $a \frac{dg}{da}$  are independent of the regularization scheme, and thus may be taken from continuum one and two loop calculations:

$$(3.39) \quad a \frac{dg}{da} = \beta_0 g^3 + \beta_1 g^5 + \cdots$$

where  $\beta_0 = \frac{1}{16\pi^2}(11 - \frac{2}{3}N_F)$  and  $\beta_1 = \frac{1}{16\pi^2}(102 - \frac{38}{3}N_F)$ . Integration of this equation

yields the desired relation

$$(3.40) \quad a(g) = \frac{1}{\Lambda_L} (\beta_0 g^2)^{-\beta_1/2\beta_0^2} e^{-1/2\beta_0 g^2}$$

where  $\Lambda_L$  is an integration constant and we have used the values of  $\beta_0$  and  $\beta_1$  for  $SU(3)$  with  $N_F$  Fermions.

The constant  $\Lambda_L$  governing the relation between the bare coupling constant and the lattice cutoff can be related by one-loop continuum calculations to the constants  $\Lambda_{\text{MOM}}$  and  $\Lambda_{\overline{MS}}$ , which govern the relation between the renormalized coupling constant and continuum cutoff using the momentum space subtraction procedure in Feynman gauge and the minimal subtraction procedure respectively, with the results [6]

$$(3.41) \quad \Lambda_{\text{MOM}} = 83.5 \Lambda_L \quad , \quad \Lambda_{\overline{MS}} = 28.9 \Lambda_L \quad .$$

This correspondence is important for two reasons. First, the large coefficients in (3.41) allow us to reconcile our notion that the basic scale  $\Lambda_{\text{QCD}}$  is of order several hundred MeV with the fact that lattice measurements yield values of  $\Lambda_L \sim 4 - 4.6$  MeV, which would otherwise appear astonishingly low. Second, in principle, it will provide a quantitative consistency test if experiments in the perturbative regime of QCD can produce sufficiently accurate values of  $\Lambda_{\text{MOM}}$  or  $\Lambda_{\overline{MS}}$ .

There is now convincing evidence that lattice calculations in the pure gauge sector display the correct renormalization group behavior, and thus provide accurate solutions of continuum QCD. Numerical evidence exists for two independent quantities,  $T_{\text{tr}}$ , the temperature of the deconfinement transition, and the string tension  $\sigma$ . The transition temperature on a lattice with  $N_t$  time slices is given by  $T_{\text{tr}} = 1/N_t a(g_{\text{tr}})$  where  $g_{\text{tr}}$  is the value of the coupling for which the transition occurs. If  $a(g_{\text{tr}})$  is calculated using the perturbative expression (3.40), then once  $g$  is small enough that the lattice theory coincides with the continuum theory, the quantity  $T_{\text{tr}}/\Lambda_L$  should approach a constant. A number of calculations show that this is the case above  $\beta = 6/g^2 = 6$ . Similarly, one observes the same behavior in the string tension by plotting  $\sigma/\Lambda_L^2$  as a function of  $\beta = 6/g^2$  and observing that this ratio approaches a constant beyond  $\beta = 6$ .

On the theoretical side, impressive progress has been made in constructing improved actions, which in addition to containing the leading order contribution to the action in Eq. 3.19, also include corrections to higher order in  $a$  (or equivalently,  $1/g^2$ ). The most straightforward corrections are calculated perturbatively, but suffer from the fact that each additional operator in field theory has its own renormalization constant, and making a 10% error by calculating such a constant perturbatively is like making 10% typing errors in the coefficients of an allegedly high-order Runge-Kutta integration formula. A more effective approach is the recent use of renormalization group methods [7] to derive nonperturbatively corrected ‘‘perfect actions’’ which provide extremely impressive approximations to the continuum theory.

In summary, lattice gauge theory in the pure gauge sector is quite satisfactory. There are no glaring conceptual or computational problems, and all the numerical evidence to

date suggests that one obtains an excellent approximation to the continuum theory for  $\beta_g$  above 6. In contrast, we will now see that full QCD including dynamical Fermions is more problematic at both the conceptual and computational levels.

#### 4. – Lattice QCD with Quarks

Significant new problems arise when one attempts to apply the ideas which are so successful for the stochastic evolution of path integrals for Bosons to many-Fermion systems. The fundamental underlying problem is the minus signs arising from antisymmetry. In the absence of projection onto the antisymmetric subspace,  $e^{-\beta H}$  filters out the lowest state of any symmetry, and favors the lowest symmetric state of energy  $E_0^S$  relative to the lowest antisymmetric state with energy  $E_0^A$  by the factor  $e^{-\beta(E_0^A - E_0^S)}$ . If one attempts to project stochastically, for example by antisymmetrizing path integral Monte Carlo evolution at each step, the projection error is of order  $1/\sqrt{N}$  and can never overcome the exponential factor in cases in which  $E_0^A$  represents a half filled band, Fermi sea, or Dirac sea and  $E_0^S$  corresponds to a Bose condensate in the lowest state. Thus, aside from special cases such as one spatial dimension, the only known alternative is to write a path integral with Grassmann variables, introduce integrals over auxiliary fields if necessary to reduce it to quadratic form, and integrate out the Fermion variables as in Eq. (2.33) to obtain a Bosonic action containing a Fermionic determinant. Since the Grassmann integral has been done analytically, the projection onto the antisymmetric space is exact, eliminating one part of the sign problem. The resulting determinant may be positive or negative, so there still remains the danger of catastrophic sign cancellations in the stochastic evaluation of the remaining Bosonic integrals. If, however, as in our present case, there is an even number of Fermion species with the same action, the determinant appears with an even power and this final sign problem is also eliminated.

This major detour to beat the Fermion sign problem comes at a high price. We started with Fermions, which in occupation number representation are represented by a bunch of 1's and 0's, and we seek to deal with them on a digital computer which can only work in terms of 1's and 0's. Yet we must resort to calculating determinants of huge, non-local, nearly-singular matrices involving exceedingly large numbers of floating-point variables and operations. In addition, by virtue of putting the Fermions on a lattice, we encounter an additional unexpected difficulty associated with Fermion doubling, which we will discuss next. It should thus be clear at the outset, that the treatment of Fermions provides fertile ground for new ideas.

**4.1. Naive Lattice Fermions and Doubling.** – To appreciate the essential issues, consider the simplest Hermitian finite difference expression with the desired continuum limit:

$$S_F^{\text{naive}} = a^4 \sum_{\vec{n}} \left[ \bar{\psi}(\vec{n}) m \psi(\vec{n}) + \frac{1}{2a} \sum_{\mu} \left\{ \bar{\psi}(\vec{n}) \gamma_{\mu} U_{\mu}(n) \psi(\vec{n} + a_{\mu}) - \bar{\psi}(\vec{n} + a_{\mu}) \gamma_{\mu} U_{\mu}^{\dagger}(n) \psi(\vec{n}) \right\} \right]$$

$$\begin{aligned}
&\implies \int d^4x \left[ \bar{\psi} m \psi + \frac{1}{2a} \sum_{\mu} \left\{ \bar{\psi} \gamma_{\mu} (1 + igA_{\mu}) (1 + a\partial_{\mu}) \psi \right. \right. \\
&\quad \left. \left. - \bar{\psi} \left( 1 + a \overleftarrow{\partial}_{\mu} \right) \gamma_{\mu} (1 - igaA_{\mu}) \psi \right\} \right] \\
(4.1) \quad &\implies \int d^4x \bar{\psi} [m + \gamma_{\mu} (\partial_{\mu} + igA_{\mu})] \psi .
\end{aligned}$$

Note that throughout we will use Euclidean  $\gamma$ -matrices satisfying  $\gamma_{\mu}\gamma_{\nu} + \gamma_{\nu}\gamma_{\mu} = 2\delta_{\mu\nu}$ , for which an explicit representation is given in Ref.[9]. Although this naive action appears to have the desired continuum behavior and symmetries, it has an unexpected problem. To see this problem in its simplest form, consider the Hamiltonian corresponding to the action (4.1) in one space dimension for the special case of free quarks ( $A = 0$ ) and zero mass:

$$\begin{aligned}
H^{\text{naive}} &= a \sum_n \psi^{\dagger}(n) \alpha \frac{1}{i2a} (\psi(n+1) - \psi(n-1)) \\
(4.2) \quad &\implies \int dx \psi^{\dagger} \alpha \frac{1}{i} \partial_x \psi
\end{aligned}$$

where  $\alpha = \gamma_0\gamma_1$  and for convenience we choose the representation  $\alpha = \begin{pmatrix} 1 & 0 \\ 0 & -1 \end{pmatrix}$ . Note that  $H^{\text{naive}}$  is Hermitian by virtue of the symmetric difference  $\psi(n+1) - \psi(n-1)$ . We now transform the field operators to momentum space by writing the Fourier sum

$$(4.3) \quad \psi(n) = \frac{1}{\sqrt{Na}} \sum_{k=-\frac{\pi}{a}}^{\frac{\pi}{a}} \psi_k e^{ikna}$$

where it is understood that for a lattice with  $N$  sites and periodic boundary conditions, the sum over momenta in the first Brillouin zone extends over the  $N$  momenta

$$(4.4) \quad k_p = \frac{p\pi}{Na} \quad -\frac{N}{2} \leq p \leq \frac{N}{2} .$$

The Hamiltonian is diagonal

$$(4.5) \quad H^{\text{naive}} = \sum_{k=-\frac{\pi}{a}}^{\frac{\pi}{a}} \psi_k^{\dagger} \alpha \frac{\sin(ka)}{a} \psi_k$$

and thus has the eigenvalue spectrum

$$(4.6) \quad E_k = \pm \frac{\sin ka}{a} \underset{k \rightarrow 0}{\sim} \pm k \left( 1 - \frac{(ka)^2}{3} + \dots \right)$$

with eigenfunctions

$$(4.7) \quad \Psi_k^{\pm}(n) = e^{ikna} \chi^{\pm}$$



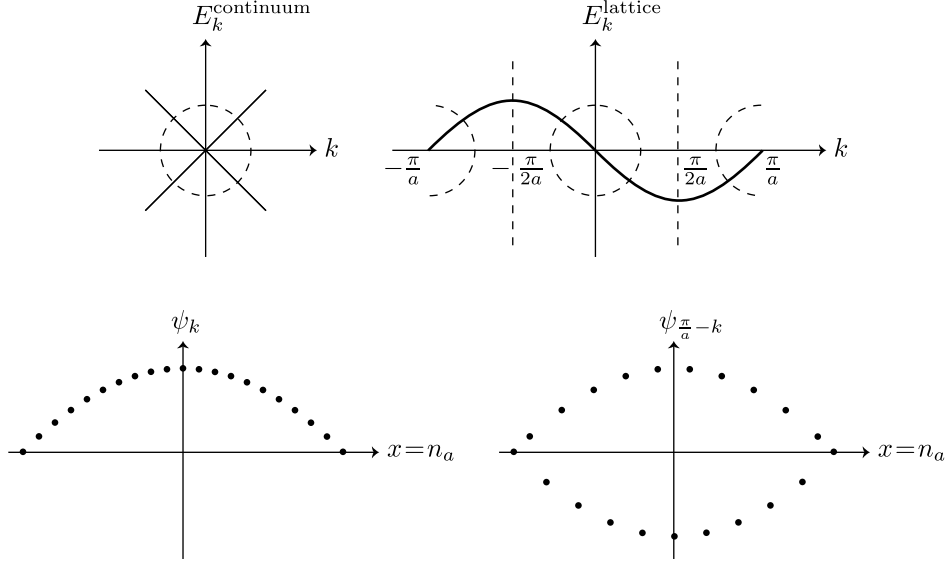


Fig. 4. – Fermion doubling in one dimension. The top plots compare the physical continuum spectrum with the spectrum of the lattice Hamiltonian. The lower plots show a half wavelength of the real part of the non-vanishing component of a physical wave function  $\Psi_k(x)$  and its degenerate unphysical sawtooth partner  $\Psi_{\frac{\pi}{a}-k}(x)$ .

where  $\chi^\pm$  is a two component spinor with either an upper or lower component unity and the other component zero. The comparison of the continuum spectrum for a massless Dirac particle  $E_k = \pm k$  and the lattice spectrum in the top of Fig. 4 displays the species doubling problem. In the region denoted by the dashed circle centered at the origin, the lattice spectrum (4.6) yields a good approximation to the linear physical spectrum, and the range of linearity increases as  $a \rightarrow 0$ . However, at the edge of the Brillouin zone, there is a second region in which the spectrum also goes to zero linearly, denoted by the two dashed semicircles. In fact, for every physical mode  $\Psi_k$ , there is a precisely degenerate unphysical mode  $\Psi_{\frac{\pi}{a}-k}$ . Since the partition function blindly counts and weights all modes according to their energies, it is clear that all Fermion loops will be overcounted by a factor of 2 in all physical observables. Note also that since the velocity is  $v = \frac{dE}{dk}$ , the lattice spectrum necessarily mixes right-moving and left-moving modes.

The origin and structure of the doubled states is simple. The degenerate partner to the state  $\Psi_k(n) = e^{ikna}\chi$  is the state  $\psi_{\frac{\pi}{a}-k}(n) = e^{in\pi}e^{-ikna}\chi$ , that is, a sawtooth mode in which every other lattice site has an extra factor of  $-1$ . The real part of a low  $k$  mode  $\Psi_k$  and its sawtooth partner  $\Psi_{\frac{\pi}{a}-k}$  are sketched for a half wavelength in the lower section of Fig. 4. Note that although there are sufficient points in the half wavelength of  $\Psi_k$  to yield an accurate integral with any smooth function, there is no way that the rapidly oscillating wave function  $\Psi_{\frac{\pi}{a}-k}$  can represent a mode with momentum

near  $\frac{\pi}{a}$ . Thus, we need some way to eliminate these modes so that they play no role in the continuum limit. The origin of the degeneracy of the physical mode with its sawtooth partner is the symmetric difference approximation to the derivative  $\psi' \sim \frac{\psi(n+1) - \psi(n-1)}{2a}$  in the naive Hamiltonian (4.2), which clearly is impervious to the minus signs  $e^{-in\pi}$  and thus yields the same magnitude for the derivatives of  $\psi_k$  and  $\psi_{\frac{\pi}{a}-k}$ . The origin of this symmetric difference, in turn, is Hermiticity, since expressions involving only nearest neighbor differences like  $\psi^\dagger n(\psi(n+1) - \psi(n))$  are non-Hermitian and yield complex eigenvalues.

We may note in passing that a finite difference approximation to a second derivative strongly breaks the degeneracy between the physical and sawtooth modes. Indeed, a perturbation of the following form

$$\begin{aligned}
 H' &= - \sum_n \psi^\dagger(n) \gamma_0 (\psi(n+1) - 2\psi(n) + \psi(n-1)) \\
 &= -a a \sum_n \psi^\dagger(n) \gamma_0 \left( \frac{\psi(n+1) - 2\psi(n) + \psi(n-1)}{a^2} \right) \\
 (4.8) \quad &\xrightarrow{a \rightarrow 0} -a \int dx \bar{\psi}(x) \psi''(x) \xrightarrow{a \rightarrow 0} 0
 \end{aligned}$$

which vanishes in the continuum limit and behaves like a momentum-dependent mass term

$$(4.9) \quad H' = \sum_k \bar{\psi}_k m(k) \psi_k$$

where

$$\begin{aligned}
 m(k) &= \frac{2}{a} (1 - \cos(ka)) \\
 &\underset{k \rightarrow 0}{\sim} ak^2 \\
 (4.10) \quad &\underset{k \rightarrow \frac{\pi}{a}}{\sim} \frac{4}{a} .
 \end{aligned}$$

For the physical modes in the region of the origin, the perturbation has no effect as  $a \rightarrow 0$ , consistent with the fact  $H'$  vanishes in the continuous limit. For the spurious sawtooth modes, however, the mass diverges as  $\frac{1}{a}$ . Thus, one way to remove the unphysical modes would be to include a term of the form (4.8) in the lattice Hamiltonian to raise their mass so high that they contribute negligibly to the partition function, and this is the idea underlying Wilson's lattice action for Fermions discussed below.

The doubling we have discussed for simplicity in one dimension arises analogously in each of the four Euclidean dimensions of the naive Fermion action, Eq. (4.1), so that we obtain  $2^4 = 16$  lattice modes for each physical mode. Again, specializing to the massless case, the momentum space action corresponding to Eq. (4.1) is

$$(4.11) \quad S_F^{\text{naive}} \equiv \bar{\psi} M \psi = \sum_k \bar{\psi}_k \sum_\mu \gamma_\mu \frac{\sin(k^\mu a)}{a} \psi_k$$

so that the inverse propagator is

$$(4.12) \quad \langle T\bar{\psi}\psi \rangle^{-1} = M(k) = \sum_{\mu} \gamma_{\mu} \frac{\sin(k^{\mu}a)}{a} .$$

This propagator replicates the physical behavior in the region of  $k^{\mu} \sim 0$  fifteen times around points on the edge of the four-dimensional Brillouin zone at which one or more of the components  $k^{\mu} \sim \frac{\pi}{a}$ .

We are now prepared to understand both the features giving rise to the doubling problem and the generality of the problem.[14] Whereas the specific function  $\sin(k^{\mu}a)$  in Eqs. (4.4a) and (4.6) is the result of using the lowest-order Hermitian difference formula for the derivatives in the continuum action, the most general form of the chiral symmetric, Hermitian action derived from discrete derivatives on a periodic lattice with the correct continuum limit is

$$(4.13) \quad S_F = \sum_k \bar{\psi}_k \sum_{\mu} \gamma_{\mu} P^{\mu}(k) \psi_k$$

where  $P^{\mu}(k)$  is real for Hermiticity,  $P^{\mu}(k) \xrightarrow[k \rightarrow 0]{} 0$  for the correct continuum limit, and  $P^{\mu}(k)$  is periodic under  $k^{\mu} \rightarrow k^{\mu} + \frac{2\pi}{a}$  and continuous for local discrete difference formulae on a lattice. Note that chiral symmetry requires the form  $\bar{\psi}\gamma_{\mu}P^{\mu}\psi$ , so that under a chiral transformation  $\psi \rightarrow e^{i\alpha\gamma_5}\psi$ , the two sign changes from  $\gamma_0$  in  $\bar{\psi}$  and  $\gamma_{\mu}$  leave the action invariant. Since  $P^{\mu}(k)$  is real, continuous and periodic in  $k^{\mu}$  with period  $\frac{2\pi}{a}$ , it must cross the axis at some intermediate point, so that this general discrete action has the doubling observed in Eq. (4.11) in each of the four Euclidean directions yielding 15 spurious low-mass excitations for each physical excitation. A rigorous version of these arguments is known as the Nielsen–Ninomiya no-go theorem,[15] which proves using homotopy theory that one cannot avoid Fermion doubling in a lattice theory which is simultaneously Hermitian, local and chiral symmetric.

An additional aspect of Fermion doubling is the absence of the axial anomaly. The axial current, which is conserved for gauge theories at the classical level but not conserved at the quantum level in the continuum theory, is conserved for naive lattice Fermions. Again, the culprits are the unphysical lattice duplicates of the physical Fermion excitations, which couple to an external axial current with the opposite chiral charge and effectively cancel the axial anomaly arising from the physical Fermions.

**4.2. Wilson Fermions.** – One of the ways out of the no-go theorem is to give up chiral symmetry and, following Wilson, add a second derivative term of the form (4.8) to raise the mass of the unphysical sawtooth modes. In one dimension, combining the naive Hamiltonian (4.2) with a multiple  $r$  of the perturbation (4.8) yields the Wilson Hamiltonian

$$(4.14) \quad \begin{aligned} H_W &= a \sum_n \psi^{\dagger}(n) \left[ \frac{\alpha}{i} \frac{(\psi(n+1) - \psi(n-1))}{2a} - \frac{ra\gamma_0}{2i} \frac{\psi(n+1) - 2\psi(n) + \psi(n-1)}{a^2} \right] \\ &= \sum_k \psi_k^{\dagger} \left[ \alpha \frac{\sin(ka)}{a} - r \frac{\gamma_0}{i} \frac{(\cos(ka) - 1)}{a} \right] \psi_k . \end{aligned}$$

Using a representation with  $\alpha = \sigma_3$  and  $-i\gamma_0 = \sigma_1$ , we obtain the energy spectrum

$$(4.15) \quad E^2 = \left( \frac{\sin(ka)}{a} \right)^2 + \left[ \frac{r}{a} (\cos(ka) - 1) \right]^2$$

with the limits

$$(4.16) \quad \begin{aligned} E &\xrightarrow[k \rightarrow 0]{} \pm k \left( 1 - \frac{1}{6} k^2 a^2 + \frac{r^2}{8} k^2 a^2 \right) \\ E &\xrightarrow[k \rightarrow \frac{\pi}{a}]{} \pm \frac{2r}{a} . \end{aligned}$$

Thus, for fixed  $r$ , the mode for  $k \sim 0$  has the correct continuum limit whereas the sawtooth mode for  $k \sim \frac{\pi}{a}$  becomes infinitely massive and decouples from the theory.

In four Euclidean dimensions, the corresponding Wilson action is

$$(4.17) \quad \begin{aligned} S_W &= -a^4 \sum_{\vec{n}} \frac{1}{2a} \sum_{\mu} [\bar{\psi}(\vec{n})(r - \gamma_{\mu})U_{\mu}(\vec{n})\psi(\vec{n} + a_{\mu}) + \bar{\psi}(\vec{n} + a_{\mu})(r + \gamma_{\mu})U_{\mu}^{\dagger}(\vec{n})\psi(\vec{n})] \\ &+ a^4 \sum_{\vec{n}} \left( m + \frac{4r}{a} \right) \bar{\psi}(\vec{n})\psi(\vec{n}) \end{aligned}$$

and the propagators for the spurious modes acquire masses which diverge as  $\frac{r}{a}$  as in the one-dimensional case.

The Wilson action manifestly breaks chiral symmetry for  $m = 0$ , since under the transformation  $\psi \rightarrow e^{i\alpha\gamma_5}\psi$ ,  $\bar{\psi}\psi \rightarrow \bar{\psi}e^{i2\alpha\gamma_5}\psi$ . As long as the contribution of the symmetry breaking term can be made arbitrarily small, its presence does not interfere with the physics of spontaneous symmetry breaking. In the case of a spin system, for example, one defines the spontaneous magnetization as the limit of the thermodynamic trace of the spin in the presence of an external magnetic field in the limit as the external field goes to zero. Heuristically, we expect the contribution of the chiral symmetry breaking term to vanish in the continuum limit even though the masses of the unphysical modes go to infinity since  $a \int dx \bar{\psi}\square^2\psi \xrightarrow[a \rightarrow 0]{} 0$ , and explicit calculation [14] shows that this is the case. Furthermore, including 15 massive Wilson Fermion partners as well as the physical mode yields the correct axial anomaly in the continuum limit.[14]

The combination  $M = \left( m + \frac{4r}{a} \right)$  in Eq. (4.17) enters the action like a mass term. Since this mass term is not protected from renormalization by any symmetry, it must be renormalized by ‘‘fine tuning.’’ Thus, by a search involving a series of calculations of the pion mass at fixed coupling constant  $g$  and Wilson  $r$ , we may determine a critical mass  $M_{\text{cr}}(g, r)$  such that  $m_{\pi} = 0$  for a chiral symmetric theory and  $M(g, r)$  such that  $m_{\pi} = 140$  MeV for the physical theory. To the extent to which it is meaningful to define a quark mass, one may define  $M_{\text{quark}} \equiv M - M_{\text{cr}}$ . A more conventional notation is in terms of the hopping parameter

$$(4.18) \quad \kappa \equiv \frac{1}{2Ma} = \frac{1}{2ma + 8r}$$

and rescaled Fermion fields

$$(4.19) \quad \Psi \equiv (Ma^4)^{1/2} \psi$$

for which the action has the form

$$(4.20) \quad S_W = \sum_{\vec{n}} \left\{ \bar{\Psi}(\vec{n})\Psi(\vec{n}) - \kappa \sum_{\mu} \left[ \bar{\Psi}(\vec{n})(r - \gamma_{\mu})U_{\mu}(\vec{n})\Psi(\vec{n} + a_{\mu}) \right. \right. \\ \left. \left. + \bar{\Psi}(\vec{n} + a_{\mu})(r + \gamma_{\mu})U_{\mu}^{\dagger}(\vec{n})\Psi(\vec{n}) \right] \right\}$$

and

$$(4.21) \quad M_{\text{quark}} = \frac{1}{2a} \left( \frac{1}{\kappa} - \frac{1}{\kappa_{\text{cr}}} \right) .$$

The fields have been scaled such that the diagonal term is now unity, and the hopping parameter  $\kappa$  specifies the strength of the nearest-neighbor coupling via link variables. Although the Wilson parameter  $r$  is often chosen to be 1, in principle it may be optimized to render the errors from  $ar\bar{\psi}\square^2\psi$  in the physical modes and the contribution of the sawtooth modes comparable.

Just as one can derive the conserved vector current of the continuum theory as the Noether current of the continuum action, one can derive a discrete version of Noether's theorem from the Wilson action (4.17) of the form

$$(4.22) \quad \Delta^{\mu} V_{\mu}(\vec{n}) \equiv V_{\mu}(\vec{n}) - V_{\mu}(\vec{n} - a_{\mu}) = 0$$

where the conserved vector current on the lattice is

$$(4.23) \quad V_{\mu}(\vec{n}) = -\frac{1}{2}\bar{\psi}(\vec{n})(r - \gamma_{\mu})U_{\mu}(\vec{n})\psi(\vec{n} + a_{\mu}) \\ + \frac{1}{2}\bar{\psi}(\vec{n} + \mu)(r + \gamma_{\mu})U_{\mu}^{\dagger}(\vec{n})\psi(\vec{n}) .$$

Note that neither the local current  $\bar{\psi}(\vec{n})\gamma_{\mu}\psi(\vec{n})$  nor the point-split current defined by (4.23) with  $r = 0$  is conserved on the lattice. In contrast, since there is no chiral symmetry, there is no unique definition of the lattice axial current, so it is necessary to use perturbation theory to explicitly calculate the difference between any choice for the lattice axial current and the continuum axial current.

In summary, Wilson Fermions provide one possible framework for solving the doubling problem on the lattice and calculations discussed subsequently will be based on this formulation. Other alternatives include staggered fermions [16], which while not avoiding the no-go theorem, maintain a remnant of chiral symmetry while thinning the spurious degrees of freedom from 16 down to 4 in four dimensions, and Kaplan-Shamir fermions [17], which are formulated on the four-dimensional boundary of a five-dimensional sphere.

**4.3. Hopping parameter expansion.** – Just as the strong-coupling expansion provided insight into the solutions of lattice QCD in the pure gauge sector, expansion in powers

of the hopping parameter,  $K$ , provides analogous insights into solutions in the presence of Fermions. The basic idea is to expand the integral

$$(4.24) \quad Z = \int \mathcal{D}(\bar{\psi}\psi)\mathcal{D}(U)e^{-\bar{\psi}(1+KU)\psi-S(U)}$$

in powers of the hopping term  $\bar{\psi}KU\psi_{n\pm 1}$ . Integration over all  $\bar{\psi}\psi$  then yields the sum of all possible closed chains of  $KU$  in which the  $U$ 's are oriented head to tail, and these closed quark paths represent all the quark time histories. As before, integrating over all  $U$  then tiles the closed quark loops with gluons, giving rise to all the color singlet flux tubes connecting the quarks and antiquarks on any time slice.

Now, consider a path integral corresponding to the propagation of a meson from space-time point  $x$  to  $y$ , which we write schematically, ignoring  $\gamma$  matrices, as

$$(4.25) \quad \begin{aligned} \langle Te^{-\beta H}\bar{\psi}_y\psi_y\bar{\psi}_x\psi_x \rangle &= Z^{-1} \int \mathcal{D}(U)\mathcal{D}(\bar{\psi}\psi)e^{-\bar{\psi}M(U)\psi-S(U)}\bar{\psi}_y\psi_y\bar{\psi}_x\psi_x \\ &= Z^{-1} \int \mathcal{D}(U)e^{\ln \det M(U)-S(U)}M_{yx}^{-1}(U)M_{xy}^{-1}(U) \end{aligned}$$

where  $M = (1 + KU)$ . Expanding  $M_{yx}^{-1}(U) = (1 + KU)_{yx}^{-1}$  in powers of  $K$  generates all valence quark trajectories from  $x$  to  $y$  and similarly  $M_{xy}^{-1}(U)$  generates trajectories from  $y$  to  $x$ .

Expansion of  $\ln \det M(U)$  generates all disconnected quark loops corresponding to excitation of quark-antiquark pairs from the Dirac sea, and expansion of  $S(U)$  tiles surfaces between these valence and sea-quark trajectories. A typical configuration showing a valence quark-antiquark pair propagating from  $x$  to  $y$ , a quark-antiquark loop excited out of the fermi sea, and a minimal tiling by plaquettes is shown in Fig. 5. Cutting this tiling at various time slices corresponds to a quark-antiquark pair connected by a flux tube or two quark-antiquark pairs connected by flux tubes. From this argument, we see that omission of the determinant, which is very expensive computationally, yields the quenched or valence approximation in which quark-antiquark pairs excited from the sea are neglected. Typical lattices used in numerical calculation vary from  $16^2 \times 32$  to  $32^3 \times 64$  sites and thus involve integration over  $10^7$  to  $10^8$  real variables.

**4.4. Correlation functions.** – As in the case of other strongly interacting many-body systems, to understand the structure of the vacuum and light hadrons in nonperturbative QCD, it is instructive to study appropriately selected ground state correlation functions, to calculate their properties quantitatively, and to understand their behavior physically.

Because of our subsequent interest in instantons, we will focus our attention on vacuum point-to-point equal time correlation functions of hadronic currents

$$(4.26) \quad R(x) = \langle \Omega | T J(x) \bar{J}(0) | \Omega \rangle$$

discussed in detail by Shuryak [1] and recently calculated in quenched lattice QCD.[18] The motivation for supplementing knowledge of hadron bound state properties by these

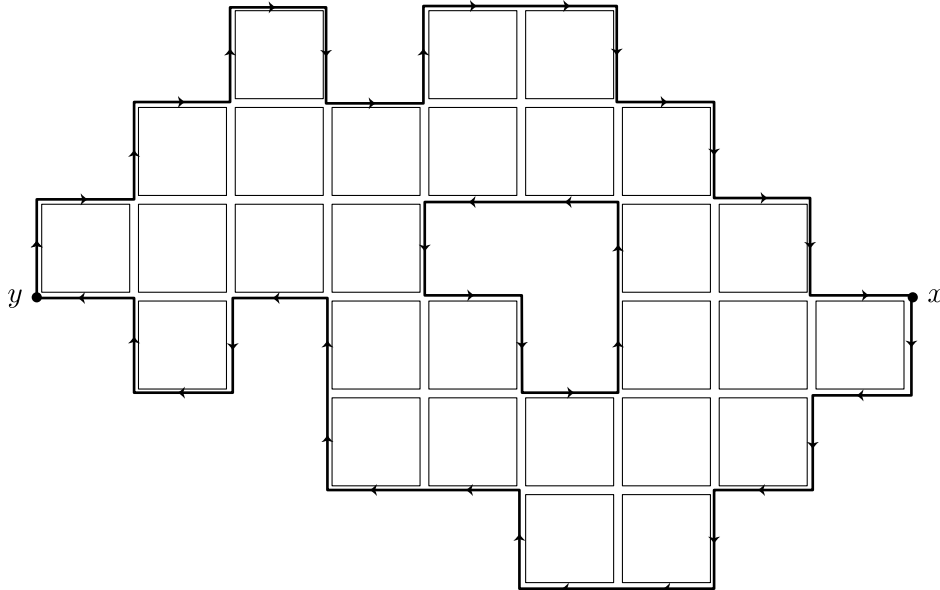


Fig. 5. – A typical time history arising in the hopping parameter expansion. The heavy lines connecting  $x$  and  $y$  denote valence quarks, the interior heavy line corresponds to a quark-antiquark pair, and the light lines denote gluons.

correlation functions is clear if one considers the deuteron. Simply knowing the binding energy, rms radius, quadruple moment and other ground state properties yields very little information about the nucleon-nucleon interaction in each spin, isospin and angular momentum channel as a function of spatial separation. To understand the nuclear interaction in detail, one inevitably would be led to study nucleon-nucleon scattering phase shifts. Although, regrettably, our experimental colleagues have been most inept in providing us with quark-antiquark phase shifts, the same physical information is contained in the vacuum hadron current correlation functions  $R(x)$ . As shown by Shuryak [1], in many channels these correlators may be determined or significantly constrained from experimental data using dispersion relations. Since numerical calculations on the lattice agree with empirical results where available, we regard the lattice results as valid solutions of QCD in all channels and thus use them to obtain information comparable to scattering phase shifts.

The correlation functions we calculate in the pseudoscalar, vector, nucleon and Delta channels are

$$\begin{aligned}
 R(x) &= \langle \Omega | T J^P(x) \bar{J}^P(0) | \Omega \rangle \\
 R(x) &= \langle \Omega | T J_\mu(x) \bar{J}_\mu(0) | \Omega \rangle \\
 R(x) &= \frac{1}{4} \text{Tr} \left( \langle \Omega | T J^N(x) \bar{J}^N(0) | \Omega \rangle x_\nu \gamma_\nu \right)
 \end{aligned}$$

and

$$R(x) = \frac{1}{4} \text{Tr} (\langle \Omega | T J_\mu^\Delta(x) \bar{J}_\mu^\Delta(0) | \Omega \rangle x_\nu \gamma_\nu )$$

where

$$\begin{aligned} J^P &= \bar{u} \gamma_5 d \\ J_\mu &= \bar{u} \gamma_\mu \gamma_5 d \\ J^N &= \epsilon_{abc} [u^a C \gamma_\mu u^b] \gamma_\mu \gamma_5 d^c \end{aligned}$$

and

$$J_\mu^\Delta = \epsilon_{abc} [u^a C \gamma_\mu u^b] u^c .$$

As in Refs. [1] and [18], we consider the ratio of the correlation function in QCD to the correlation function for non-interacting massless quarks,  $R(x)/R_0(x)$ , which approaches one as  $x \rightarrow 0$  and displays a broad range of non-perturbative effects for  $x$  of the order of 1 fm. Typical results of lattice calculations of ratios of vacuum correlation functions are shown in Fig. 6.

Note that the lattice results (solid line) agree well with phenomenological results from dispersion analysis of data (long dashed curves). Also, observe that the vector and pseudoscalar correlation functions are strongly dominated by the rho and pion contributions (dotted lines) in the region of 0.5 to 1.5 fm. We will subsequently show that these rho and pion contributions in turn arise from the zero mode contributions associated with instantons.

As discussed in Refs. [1, 18], these vacuum correlators show strong indications of instanton dominated physics. As shown by 't Hooft [19], the instanton induced interaction couples quarks and antiquarks of opposite chirality leading to strong attractive and repulsive forces in the pseudoscalar and scalar channels respectively and no interaction to leading order in the vector channel. Just this qualitative behavior is observed at short distance in all the channels we computed. Furthermore, as shown by the open circles with error bars in Fig. 6, the random instanton model of Shuryak et al. [2] reproduces the main features of the correlation functions at large distance as well.

## 5. – The Role of Instantons in Light Hadrons

Having established the framework of lattice QCD, I will now use it as a tool to elucidate the role of instantons in light hadrons. The QCD vacuum is understood as a superposition of an infinite number of states of different winding number, where the winding number characterizes the number of times the group manifold is covered when one covers the physical space. Just as there is a stationary point in the action of the Euclidean Feynman path integral for a double well potential corresponding to the tunneling between the two degenerate minima, so also there is a classical solution to the QCD equations in Euclidean time, known as an instanton [20], which describes tunneling between two vacuum states of differing winding number. The action associated with an



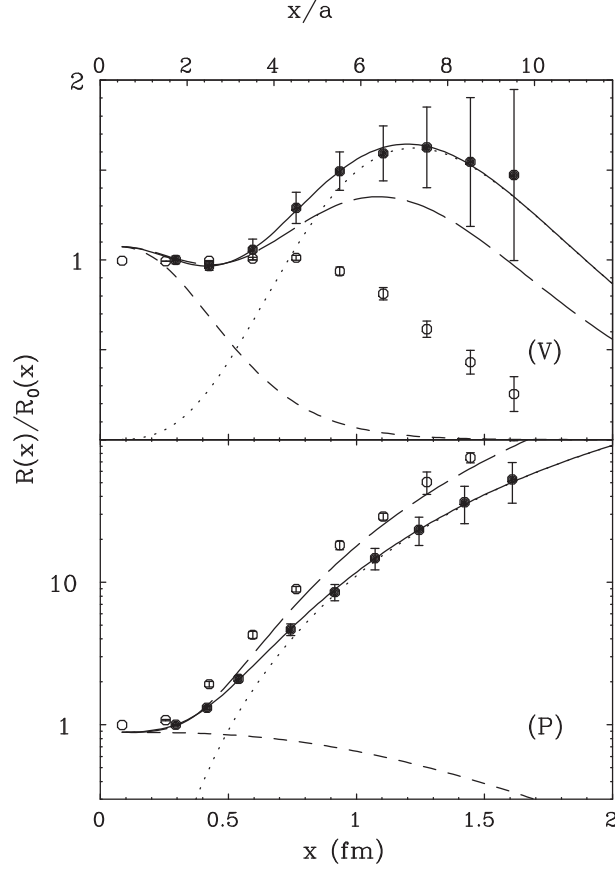


Fig. 6. – Vector (V) and Pseudoscalar (P) correlation functions are shown in the upper and lower panels respectively. Lattice results [18] are denoted by the solid points with error bars and fit by the solid curves, which may be decomposed into continuum and resonance components denoted by short dashed and dotted curves respectively. Phenomenological results determined by dispersion analysis of experimental data in Ref. [1] are shown by long dashed curves, and the open circles denote the results of the random instanton model of Ref. [2].

instanton is

$$(5.1) \quad S_0 = \frac{1}{4} \int d^4x F_{\mu\nu}^a F_{\mu\nu}^a = \frac{48}{g^2 \rho^4} \int d^4x \left( \frac{\rho^2}{x^2 + \rho^2} \right)^4 = \frac{8\pi^2}{g^2} .$$

Note that the action density has a universal shape characterized by a size  $\rho$ , and that the action is independent of  $\rho$ . Furthermore, the instanton field strength is self-dual, *i.e.*  $\tilde{F}_{\mu\nu}^a \equiv \epsilon_{\mu\nu\alpha\beta} F_{\alpha\beta}^a = \pm F_{\mu\nu}^a$ , so that the topological change of an instanton is

$$(5.2) \quad Q \equiv \frac{g^2}{8\pi^2} \frac{1}{4} \int d^4x \tilde{F}_{\mu\nu}^a F_{\mu\nu}^a = \pm 1 .$$

Two features of instantons are particularly relevant to light hadron physics. The first is the fact that although the fermion spectrum is identical at each minimum of the vacuum, quarks of opposite chirality are raised or lowered one level between adjacent minima. Thus, an instanton absorbs a left-handed quark of each flavor and emits a right-handed quark of each flavor, and an anti-instanton absorbs right-handed quarks and emits left-handed quarks. Omitting heavier quarks for simplicity, the resulting 't Hooft interaction involving the operator  $\bar{u}_R u_L \bar{d}_R d_L \bar{s}_R s_L$  is the natural mechanism to describe otherwise puzzling aspects of light hadrons. It is the natural mechanism to flip the helicity of a valence quark and transmit this helicity to the glue and quark-antiquark pairs, thereby explaining the so-called “spin crisis.” It also explains why the two valence  $u$  quarks in the proton would induce twice as many  $\bar{d}d$  pairs as the  $\bar{u}u$  pairs induced by the single valence  $d$  quark. The second feature is that each instanton gives rise to a localized zero mode of the Dirac operator  $D_\mu \gamma_\mu \phi_0(x) = 0$ . Hence, considering a spectral representation of the quark propagator, it is natural that the propagator for the light quarks is dominated by these zero modes at low energy. This gives rise to a physical picture in which  $\bar{q}q$  pairs propagate by “hopping” between localized modes associated with instantons.

**5.1. Identifying instantons by cooling.** – The Feynman path integral for a quantum mechanical problem with degenerate minima is dominated by paths that fluctuate around stationary solutions to the classical Euclidean action connecting these minima.[8] In the case of the double well potential, a typical Feynman path is composed of segments fluctuating around the left and right minima joined by segments crossing the barrier. If one had such a trajectory as an initial condition, one could find the nearest stationary solution to the classical action numerically by using an iterative local relaxation algorithm. In this method, which has come to be known as cooling, one sequentially minimizes the action locally as a function of the coordinate on each time slice and iteratively approaches a stationary solution. In the case of the double well, the trajectory approaches straight lines in the two minima joined by kinks and anti-kinks crossing the barrier and the structure of the trajectory can be characterized by the number and positions of the kinks and anti-kinks.

In QCD, the corresponding classical stationary solutions to the Euclidean action for the gauge field connecting degenerate minima of the vacuum are instantons, and we apply the analogous cooling technique [21] to identify the instantons corresponding to each gauge field configuration.

The results of using 25 cooling steps as a filter to extract the instanton content of a typical gluon configuration are shown in Fig. 7, taken from Ref. [22] using the Wilson action on a  $16^3 \times 24$  lattice at  $6/g^2 = 5.7$ . As one can see, there is no recognizable structure before cooling. Large, short wavelength fluctuations of the order of the lattice spacing dominate both the action and topological charge density. After 25 cooling steps, three instantons and two anti-instantons can be identified clearly. The action density peaks are completely correlated in position and shape with the topological charge density peaks for instantons and with the topological charge density valleys for anti-instantons. Note that both the action and topological charge densities are reduced by more than

two orders of magnitude so that the fluctuations removed by cooling are several orders of magnitude larger than the topological excitations that are retained.

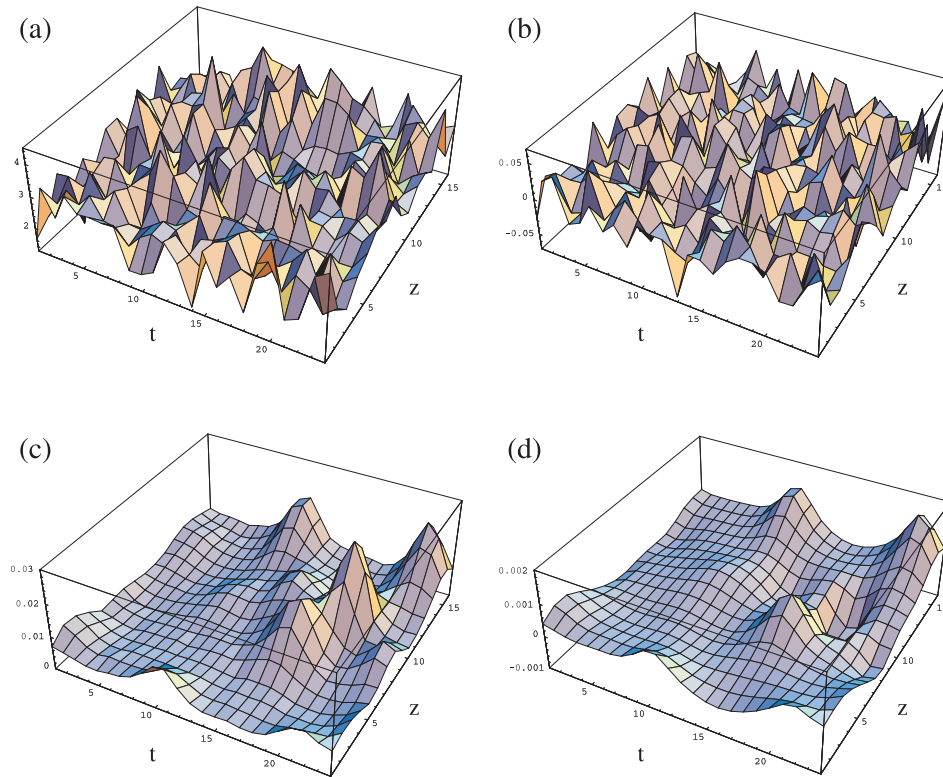


Fig. 7. – Instanton content of a typical slice of a gluon configuration at fixed  $x$  and  $y$  as a function of  $z$  and  $t$ . The left column shows the action density  $S(1, 1, z, t)$  before cooling (a) and after cooling for 25 steps (c). The right column shows the topological charge density  $Q(1, 1, z, t)$  before cooling (b) and after cooling for 25 steps.

Setting the coupling constant, or equivalently, the lattice spacing, and quark mass by the nucleon and pion masses in the usual way, it turns out that the characteristic size of the instantons identified by cooling is  $0.36 \text{ fm}$  and the density is  $1.6 \text{ fm}^{-4}$ , in reasonable agreement with the value of  $0.33 \text{ fm}$  and  $1.0 \text{ fm}^{-4}$  in the liquid instanton model.[2]

**5.2. Comparison of results with all gluons and with only instantons.** – One dramatic indication of the role of instantons in light hadrons is to compare observables calculated using all gluon contributions with those obtained using only the instantons remaining after cooling. Note that there are truly dramatic differences in the gluon content before

and after cooling. Not only has the action density decreased by two orders of magnitude, but also the string tension has decreased to 27% of its original value and the Coulombic and magnetic hyperfine components of the quark-quark potential are essentially zero. Hence, for example, the energies and wave functions of charmed and  $B$  mesons would be drastically changed.

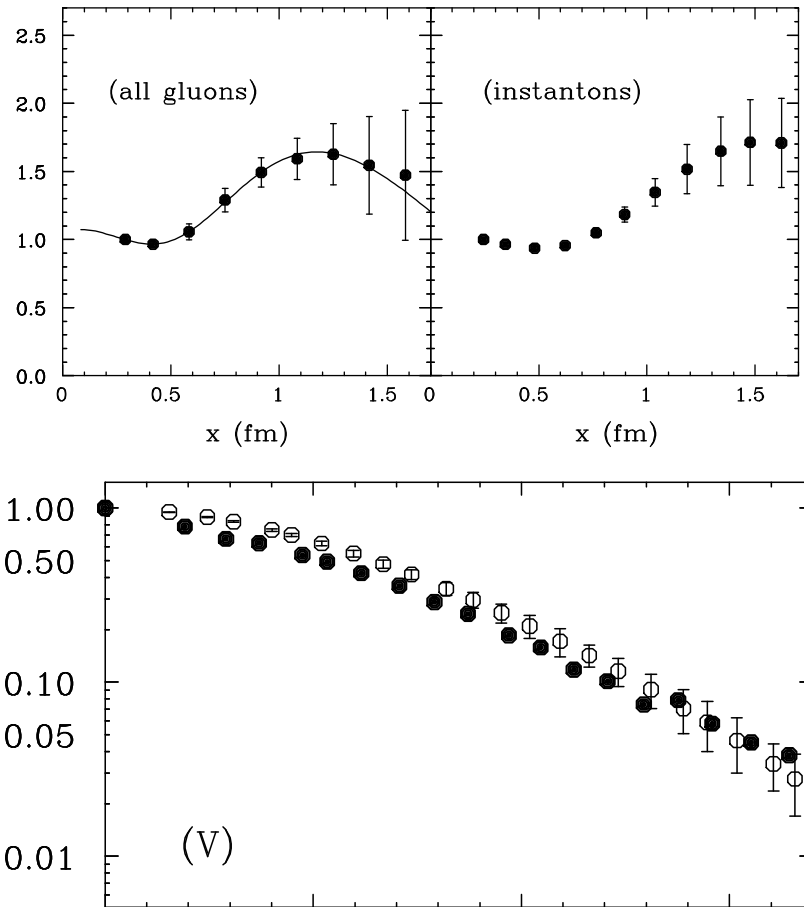


Fig. 8. – Comparison of rho observables calculated with all gluon configurations and only instantons. The upper left-hand plot shows the vacuum correlator in the rho channel calculated with all gluons as in Fig. 6 and the upper right-hand plot shows the analogous result with only instantons. The lower plot shows the ground state density-density correlation function for the rho with all gluons (solid circles) and with only instantons (open circles). Error bars for the solid circles are comparable to the open circles and have been suppressed for clarity.

As shown in Fig. 8, however, the properties of the rho meson are virtually unchanged. The vacuum correlation function in the rho (vector) channel and the spatial distribution

of the quarks in the rho ground state, given by the ground state density-density correlation function [23]  $\langle \rho | \bar{q} \gamma_0 q(x) \bar{q} \gamma_0 q(0) | \rho \rangle$ , are statistically indistinguishable before and after cooling. Also, as shown in Ref. [22], the rho mass is unchanged within its 10% statistical error. In addition, the pseudoscalar, nucleon, and delta vacuum correlation functions and nucleon and pion density-density correlation functions are also qualitatively unchanged after cooling, except for the removal of the small Coulomb induced cusp at the origin of the pion.

Although these cooling studies strongly indicate that instantons play an essential role in light quark physics, cooling has the disadvantage of modifying the instanton content of the original gluon configuration. It is possible to avoid the gradual shrinkage of a single instanton until it eventually falls through the lattice by using an improved action that is sufficiently scale independent.[24] However, pairs of instantons and anti-instantons will eventually attract each other and annihilate, thereby continually eroding the original distribution. Hence, it is valuable to complement these cooling calculations by studies of the zero modes associated with instantons, which, as we show in the next section, can be carried out successfully on the original uncooled gluon configurations.

**5.3. Eigenmodes of the Dirac operator.** – In the continuum limit, the Dirac operator for Wilson fermions approaches the familiar continuum result

$$(5.3) \quad \begin{aligned} D\psi_x &= \psi_x - \kappa \sum_{\mu} \left[ (r - \gamma_{\mu}) u_{x,\mu} \psi_{x+\mu} + (r + \gamma_{\mu}) u_{x-\mu,\mu}^{\dagger} \psi_{x-\mu} \right] \\ &\rightarrow \frac{1}{m} [m + i(\not{p} + g\not{A})] \psi . \end{aligned}$$

In the free case, the continuum spectrum is  $\frac{1}{m}[m + i|\vec{p}|]$  and the Wilson lattice operator approximates this spectrum in the physical regime and pushes the unphysical fermion modes to very large (real) masses. In the presence of an instanton of size  $\rho$  at  $x = 0$ , it is shown in Ref. [25] that the lattice operator produces a mode with zero imaginary part that approaches the continuum result

$$(5.4) \quad \psi_0(x)_{s,\alpha} = u_{s,\alpha} \frac{\sqrt{2}}{\pi} \frac{\rho}{(x^2 + \rho^2)^{3/2}}$$

and whose mixing with other modes goes to zero as the lattice volume goes to infinity. In addition, instanton-anti-instanton pairs that interact sufficiently form complex conjugate pairs of eigenvalues that move slightly off the real axis. Thus, by observing the Dirac spectrum for a lattice gluon configuration containing a collection of instantons and anti-instantons, it is possible to identify zero modes directly in the spectrum.

Fig. 9 shows the lowest 64 complex eigenvalues of the Dirac operator on a  $16^4$  unquenched gluon configuration for  $6/g^2 = 5.5$  and  $\kappa = 0.16$ , both before and after cooling (where 100 relaxation steps with a parallel algorithm are comparable to 25 cooling steps). The lower, cooled, plot has just the structure we expect with a number of isolated instantons with modes on the real axis and pairs of interacting instantons slightly off the real axis. However, even though the uncooled case shown in the upper plot also contains

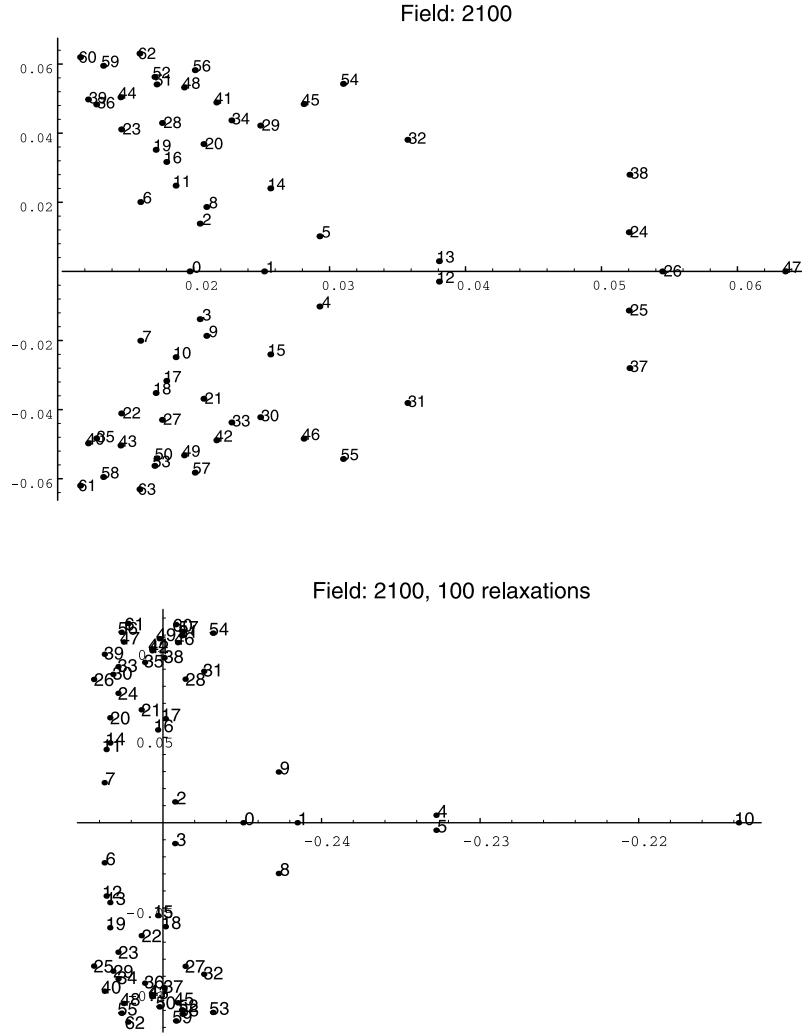


Fig. 9. – Lowest 64 complex eigenvalues of the Wilson–Dirac operator for an unquenched gluon configuration both before (upper plot) and after cooling (lower plot). The scale is such that 0.06 on the imaginary axis roughly corresponds to the lowest Matsubara frequency, 380 MeV.

fluctuations several orders of magnitude larger than the instantons (as seen in Fig. 7), it shows the same structure of isolated instantons and interacting pairs. To set the scale, note that if we had antiperiodic boundary conditions in time, the lowest Matsubara mode ( $ip = i\frac{\pi}{T}$ ) would occur at 0.06 on the imaginary axis, so all the modes below this value are presumably the results of zero modes.

**5.4. Zero mode expansion.** – The Wilson–Dirac operator has the property that  $D = \gamma_5 D^\dagger \gamma_5$ , which implies that  $\langle \psi_j | \gamma_5 | \psi_i \rangle = 0$  unless  $\lambda_i = \lambda_j^*$  and we may write the spectral representation of the propagator

$$\langle x | D^{-1} | y \rangle = \sum_i \frac{\langle x | \psi_i \rangle \langle \psi_i | \gamma_5 | y \rangle}{\langle \psi_i | \gamma_5 | \psi_i \rangle \lambda_i}$$

where  $\lambda_i = \lambda_i^*$ . A clear indication of the role of zero modes in light hadron observables is the degree to which truncation of the expansion to the zero mode zone reproduces the result with the complete propagator.

Fig. 10 shows the result of truncating the vacuum correlation functions for the vector and pseudoscalar channels to include only low eigenmodes.[25] On a  $16^4$  lattice, the full propagator contains 786,432 modes. The top plot of Fig. 10 shows the result of including the lowest 16, 32, 64, 96, and finally 128 modes. Note that the first 64 modes reproduce most of the strength in the rho resonance peak pointed out in Fig. 6, and by the time we include the first 128 modes, all the strength is accounted for. Similarly, the lower plot in Fig. 10 shows that the lowest 128 modes also account for the analogous pion contribution to the pseudoscalar vacuum correlation function. Thus, without having to resort to cooling, by looking directly at the contribution of the lowest eigenfunctions, we have shown that the zero modes associated with instantons dominate the propagation of rho and pi mesons in the QCD vacuum.

**5.5. Localization.** – Finally, it is interesting to ask whether the lattice zero mode eigenfunctions are localized on instantons. This was studied by plotting the quark density distribution for individual eigenmodes in the  $x$ - $z$  plane for all values of  $y$  and  $t$ , and comparing with analogous plots of the action density. As expected, for a cooled configuration the eigenmodes correspond to linear combinations of localized zero modes at each of the instantons. (Because there are no symmetries, the coefficients are much more complicated than the even and odd combinations in a double well or the Bloch waves in a periodic potential.) What is truly remarkable, however, is that the eigenfunctions of the uncooled configurations also exhibit localized peaks at locations at which instantons are identified by cooling. Thus, in spite of the fluctuations several orders of magnitude larger than the instanton fields themselves, the light quarks essentially average out these fluctuations and produce localized peaks at the topological excitations.

## 6. – Conclusion

Taken as a whole, lattice calculations now provide strong evidence that instantons play a dominant role in quark propagation in the vacuum and in light hadron structure. The instanton content of gluon configurations has been extracted by cooling, and the instanton size and density are consistent with the instanton liquid model. Vacuum correlation functions, ground state density-density correlation functions, and masses calculated with only instantons show striking agreement with the results obtained with all gluons. Zero modes associated with instantons are clearly evident in the Dirac spectrum,

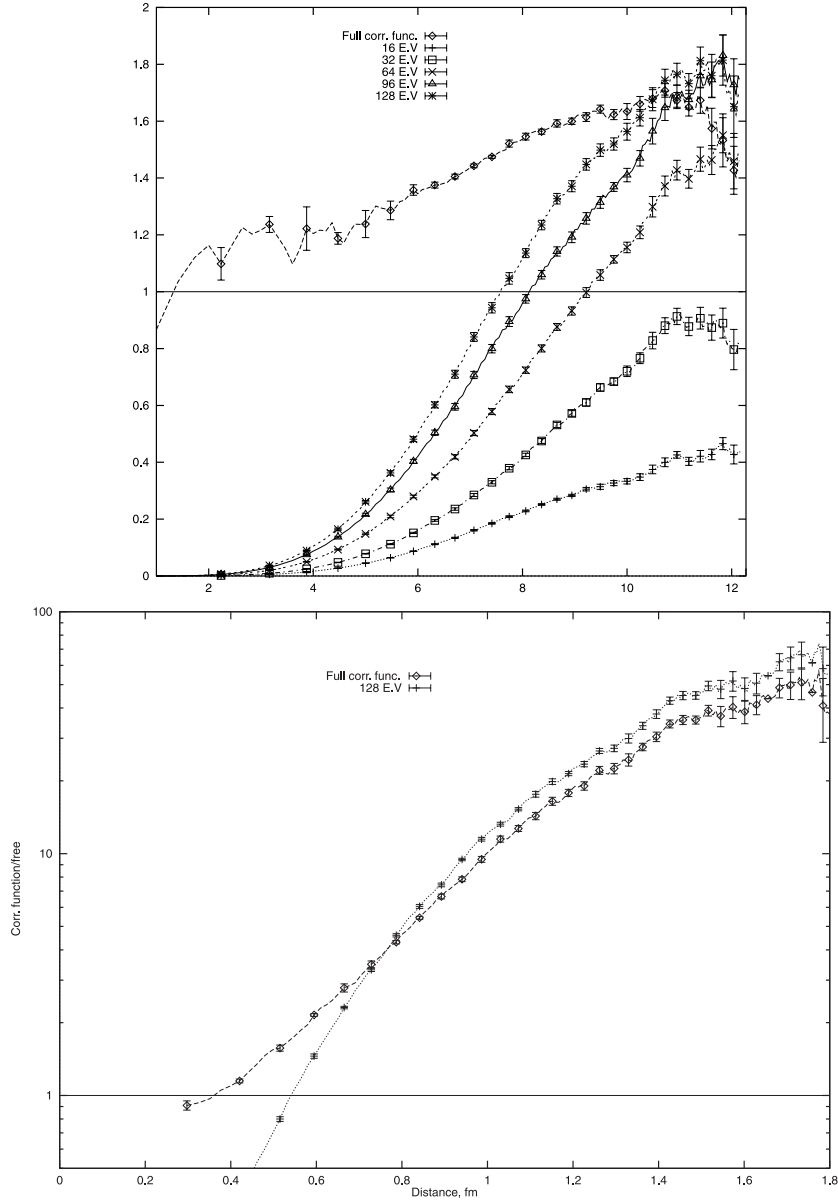


Fig. 10. – Contributions of low Dirac eigenmodes to the vector (upper graph) and pseudoscalar (lower graph) vacuum correlation functions. The upper graph shows the contributions of 16, 32, 64, 96, and 128 eigenmodes compared with the full correlation function for an unquenched configuration with a 63 MeV valence quark mass. The lower graph compares 128 eigenmodes with the full correlation function for a quenched configuration with a 23 MeV quark mass.



and account for the rho and pi contributions to vector and pseudoscalar vacuum correlation functions. Finally, quark localization at instantons has been observed directly in uncooled configurations. Hence, in addition to providing a powerful tool for calculating a variety of important physical observables, ranging from spectroscopy and weak matrix elements to QCD thermodynamics, Lattice QCD is also beginning to teach us the underlying physics of hadron structure, bit by bit.

\* \* \*

It is a pleasure to thank Professor Alfredo Molinari and Professor Renato Ricci for their hospitality at Varenna and to acknowledge the essential role of Richard Brower, Ming Chu, Jeff Grandy, Suzhou Huang, Taras Ivanenko, Kostas Orginos, and Andrew Pochinsky who collaborated in various aspects of this work. We are also grateful for the donation by Sun Microsystems of the 24 Gflops E5000 SMP cluster on which the most recent calculations were performed and the computer resources provided by NERSC with which this work was begun. This work is supported in part by funds provided by the US Department of Energy (DOE) under cooperative research agreement #DF-FC02-94ER40818.

#### REFERENCES

- [1] Shuryak E.V., *Rev. Mod. Phys.* **65**, 1 (1993), *Nucl. Phys. B* (Proc. Suppl.) **34**, 107 (1994), and Schäffer T., and Shuryak E.V., hep-ph/9610451v2.
- [2] Shuryak E.V., and Verbaarschot J.J.M., *Nucl. Phys.* **B410**, 55 (1993); Schäffer T., Shuryak E.V., and Verbaarschot J.J.M., *Nucl. Phys.* **B412**, 143 (1994).
- [3] Dyakanov D.I., and Petrov V. Yu, *Nucl. Phys.* **B245**, 259 (1984); **B272**, 457 (1986).
- [4] Gross D., and Wilczek F., *Phys. Rev.* **D9**, 980 (1974).
- [5] Ji X., Tang J., and Hoodbhoy P., *Phys. Rev. Lett.* **76**, 740 (1996).
- [6] Dashen R. and Gross D.J., *Phys. Rev.* **D23**, 2340 (1981).
- [7] Hasenfratz P. and Niedermayer F., *Nucl. Phys.* **B414**, 785 (1994); Bietenholz W. and Wiese U.-J., *Nucl. Phys.* **B464**, 319 (1996).
- [8] Negele J.W., and Orland H., *Quantum Many-Particle Systems*, New York: Addison-Wesley, 1987.
- [9] Creutz M, *Quarks, Gluons and Lattices*, Cambridge: Cambridge Univ Pr, 1983.
- [10] *Lattice Gauge Theories and Monte Carlo Simulations*, Rebbi C., ed. Singapore: World Scientific, 1983.
- [11] Rothe H., *Lattice Gauge Theories: An Introduction*, World Scientific, 1992.
- [12] Montvay I and Münster G, *Quantum Fields on a Lattice*, Cambridge: Cambridge Univ Pr, 1994.
- [13] Sharpe S., in *Phenomenology and Lattice QCD*, Kilcup G. and Sharpe S., eds. World Scientific, 1993.
- [14] Karsten L.H. and Smit J., *Nucl. Phys.* **B183**, 103 (1981).
- [15] Nielsen H.B. and Minomiya M., *Nucl. Phys.* **B185**, 20 (1981).
- [16] Kogut J. and Susskind L., *Phys. Rev.* **D11**, 395 (1975).
- [17] Kaplan D.B., *Phys. Lett.* **B288**, 342 (1992); Furman V. and Shamir Y., *Nucl. Phys.* **439**, 54 (1995).

- [18] Chu M.-C., Grandy J.M., Huang S., and Negele J.W., *Phys. Rev. Lett.* **70**, 225 (1993); *Phys. Rev.* **D48**, 3340 (1993).
- [19] 't Hooft G. *Phys. Rev.* **14D**, 3432 (1976).
- [20] Belavin A.A., Polyakov A.M., Schwartz A.P., and Tyupkin Y.S. *Phys. Lett.* **59B**, 85 (1975).
- [21] Berg B. *Phys. Lett.* **104B**, 475 (1981); Teper M., *Nucl. Phys. B* (Proc. Suppl.) **20**, 159 (1991).
- [22] Chu M.-C., Grandy J.M., Huang S., and Negele J.W., *Phys. Rev.* **D49**, 6039 (1994).
- [23] Chu M.-C., Lissia M., and Negele J.W., *Nucl. Phys.* **B360**, 31 (1991); Lissia M., Chu M.-C., Negele J.W., and Grandy J.M., *Nucl. Phys.* **A555**, 272 (1993).
- [24] de Forcrand P., Garcia Pérez M., and Stamatescu I.-O., hep-lat/9701012 (1997).
- [25] Ivanenko T., and Negele J.W., *Proceedings of Lattice '97*, to be published in *Nucl. Phys.*, hep-lat/9709130; Ivanenko T., MIT Ph.D. dissertation 1997.